A Monte Carlo simulation of neutral-current deep inelastic scattering in parton model

Master's thesis, 23.6.2022

Author:

Joni Laulainen

Supervisor:

Ilkka Helenius

UNIVERSITY OF JYVÄSKYLÄ
DEPARTMENT OF PHYSICS

Abstract

Laulainen, Joni
A Monte Carlo simulation of neutral-current deep inelastic scattering in parton model
Masters thesis
Department of Physics, University of Jyväskylä, 2022, 54 pages.

With the aim to simulate the neutral-current deep inelastic electron-proton scattering using Monte Carlo methods, the differential cross section is derived in the leading order of perturbative quantum chromodynamics. Making use of Monte Carlo sampling from a distribution, the Lorentz-invariant quantities x and Q^2 are drawn from the cross section, and the kinematics of the scattering process built. The final state particles are used to gather distributions of invariant mass W, inelasticity y and transverse momentum p_{T}. The results are compared to distributions from PYTHIA event generator for a similar collision event setup. Distributions with massless quarks agree, but adding masses to the quarks results in greater differences between the distributions.

Keywords: Deep inelastic scattering, Monte Carlo, simulation

Tiivistelmä

Laulainen, Joni
Syvästi epäelastisen sironnan neutraalin virran Monte Carlo -simulaatio partonimallissa
Pro gradu -tutkielma
Fysiikan laitos, Jyväskylän yliopisto, 2022, 54 sivua

Työn tavoitteena on simuloida syvästi epäelastista elektroni-protoni -sirontaa hyödyntäen Monte Carlo -menetelmiä. Prosessin differentiaalinen vaikutusala johdetaan häiriöteoreettisen kvanttiväridynamiikan ensimmäisessä kertaluvussa. Lorentz-invariantit suureet x ja Q^2 poimitaan vaikutusalasta käyttäen Monte Carlo -valintaa jakaumasta, ja sirontaprosessin kinematiikka rakennetaan. Lopputilan hiukkasia käyttämällä kerätään jakaumat invariantista massasta W, epäelastisuudesta y ja poikittaisliikemäärästä p_{T}. Tulokset vastaavat samanlaisen törmäysasetelman jakaumia PYTHIA-eventtigeneraattorista massattomien kvarkkien tapauksessa, mutta massojen lisääminen aiheuttaa eroavaisuuksia jakaumien välillä.

Avainsanat: Syvästi epäelastinen sironta, Monte Carlo, simulaatio

Contents

1 Introduction

The study of deep inelastic scattering (DIS) is a field of high-energy physics, which has proved successful in making advancements to the Standard Model. Electron-proton collision experiments have contributed to the discovery of quarks and the field theory of quantum chromodynamics (QCD) which describes their strong interactions. In these experiments, high-energy beams of leptons and hadrons are collided to reach a high resolution, which allows the lepton to interact with the constituent parts inside the hadron. These constituents, called partons, are described by parton distribution functions (PDFs) which are one of the main interests of the experiments. The theory which portrays the structure of the proton as a collection of these partons is the parton model.

The experiments of electron-proton DIS have been carried out in DESY-HERA collider collaborations H1 and ZEUS [1]. The experiments handled collisions in a wide range of four-momentum transfer squared, Q^2, and Bjorken x, which in the parton model is the fraction of nucleons momentum carried by the quark. Their work set the *ep* DIS as a crucial part of modern high-energy physics, with noteworthy impact on the physics of parton distributions, confirmation on quark charge fractions and the electroweak theory as a viable description of cross sections up to $Q^2 \sim M_Z^2$. [2, 3]

As the scattering processes have a quantum mechanical nature, an element of randomness is evident. This makes it feasible to simulate the processes with the use of Monte Carlo (MC) techniques, which rely on probabilistic measures and pseudorandom numbers. Monte Carlo event generators aim to produce events, interactions of two initial state particles resulting in a set of outgoing particles, which imitate the behaviour of real scattering experiment data [4]. The generators provide physicists with better understanding of the events, and can be of help in designing the experimental setups of scattering experiments. One such event generator is PYTHIA. It is a general purpose Monte Carlo event generator, capable of describing high-energy collisions of various processes [5, 6, version 8.307].

A simulation of unpolarized neutral-current *ep* DIS is carried out with the use

of MC methods. The neutral-current (NC) cross section σ, which is proportional to reaction frequency and that way analogous to scattering probability, is used as the basis of the MC sampling. The NC interactions involve electrons and protons interacting via a photon or a Z boson propagator. It can be derived in the leading order of perturbative QCD and presented in terms of structure functions, which are proportional to PDFs. In the parton level, the electron is depicted to interact with a parton, a quark or an antiquark. The scattering sub-process of elastic electron-quark scattering can be constructed with two independent variables, x and Q^2. These variables are picked from the cross section with MC sampling methods, and the final-state electron and quark are produced. Outside of parton level, as the proton breaks down, it emits new particles in the process of hadronization. The simulation used is focused only on the hard parton level process and doesn't involve hadronization. However, the scattered electron carries enough information to give access to many quantities of interest and which can be compared to results from the PYTHIA event generator.

2 Theoretical background

In the scattering process, the highly energetic electron has a wavelength of $\lambda = 1/q$, where q is its four-momentum. This is de Broglie wavelength in natural units, which we are using. As the proton's effective radius is about 1 femtometer, or 10^{-15} m, the wavelength has to be smaller than that to resolve the internal structure. This is achieved with a propagator 4-momentum q larger[1] than 0.197 GeV. Since the wavelength is significantly smaller than the apparent size of the proton, the electron can interact with the constituents of the proton. Some concepts, physical quantities and calculation methods are needed to build the simulation of this process. An important quantity, in both the theory and the experiments, is the cross section σ. It is related to the scattering probability and is often given in terms of scattering angles, particle energies, propagator virtuality Q^2 or momentum fraction of the parton x. Many of the quantities are frame-dependent, but are more easily calculated in the target rest frame (TRF), where the proton is stationary. The expression for σ is built with the use of relativistic kinematics, Lorentz-invariant quantities and the Feynman rules.

[1]The conversion is $\hbar c = 1.97 \times 10^{-16}$ m from natural units to SI units. From GeV^{-1} to fm the conversion is then 1 $\text{GeV}^{-1} = 0.197$ fm.

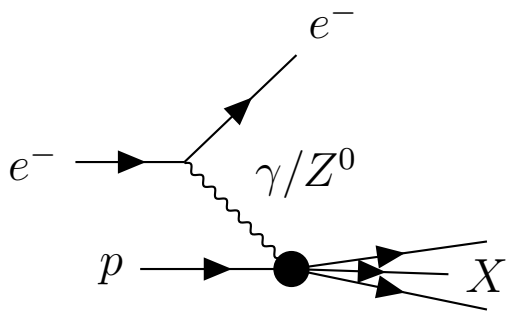

Figure 1. Feynman diagram of neutral-current ep deep inelastic scattering. The electron e^- interacts with the proton p via a photon γ or a Z boson. The proton breaks down into particles denoted by X.

2.1 Definition of cross section

Considering a scattering process with initial state particles a and b and final state particles c and $i \in [1, n]$, the cross section is experimentally defined as

$$\sigma = \frac{W}{J_a N_b} = \frac{1}{\frac{2E_a}{V}\vec{v}_a \frac{2E_b}{V} V} \frac{N_{scatt}}{\Delta T}, \tag{1}$$

where $W = N_{scatt}/\Delta T$ is reaction frequency, $J_a \overset{TRF}{=} n_a|\vec{v}_a| = 2E_a|\vec{v}_a|/V$ flux of incoming beam particles and $N_b = n_b V \overset{TRF}{=} 2E_b$ the number of target particles[2].

Using transition amplitude and the density of states to write the scattering number as $N_{scatt} = |T_{fi}|^2 \times$ (number of possible final states) with

$$|T_{fi}|^2 = \frac{1}{V^{(n+1)+2}} \Delta T V (2\pi)^4 \delta^{(4)}(p_a + p_b - p_c - \sum p_i) |\mathcal{M}|^2 \tag{2}$$

leads to differential cross section

$$d\sigma = \frac{1}{\frac{2E_a}{V}\vec{v}_a \frac{2E_b}{V}} \frac{1}{V^{(n+1)+2}} (2\pi)^4 \delta^{(4)}(p_a + p_b - p_c - \sum p_i) |\mathcal{M}|^2 \frac{V d^3 p_c}{2E_c (2\pi)^3} \prod_{i=1}^{n} \frac{V d^3 p_i}{2E_i (2\pi)^3}. \tag{3}$$

The differential cross section can be written as

$$d\sigma = \frac{\overline{|\mathcal{M}|^2}}{F} d(\mathrm{PS})_{n+1}, \tag{4}$$

where F is the flux factor and $d(\mathrm{PS})_{n+1}$ the differential phase space element of $n+1$

[2] $2E$ particles in volume V is a standard normalization in particle physics.

particles. We can identify this form in equation (3) by denoting

$$F = n_a n_b v_{ab} = 4E_a E_b |\vec{v}_a - \vec{v}_b| \overset{TRF}{=} 4E_a E_b |\vec{v}_a| = 4ME_a = 4(k \cdot p) \tag{5}$$

$$d(\mathrm{PS})_{n+1} = (2\pi)^4 \delta^{(4)}(p_a + p_b - p_c - \sum_{j=1}^{n} p_j) \frac{d^3 p_c}{2E_c (2\pi)^3} \prod_{i=1}^{n} \frac{d^3 p_i}{2E_i (2\pi)^3}. \tag{6}$$

Considering unpolarized scattering, which allows all different final state polarizations and spins, the amplitude has to be averaged over initial state spins s_n and summed over final state spins s_m as

$$\overline{|\mathcal{M}|^2} = \frac{1}{2n} \sum_{s_n} \sum_{s_m} |\mathcal{M}|^2 \text{ so that}$$

$$d\sigma = \frac{\overline{|\mathcal{M}|^2}}{4(k \cdot p)} (2\pi)^4 \delta^{(4)}(p_a + p_b - p_c - \sum_{j=1}^{n} p_j) \frac{d^3 p_c}{2E_c (2\pi)^3} \prod_{i=1}^{n} \frac{d^3 p_i}{2E_i (2\pi)^3}. \tag{7}$$

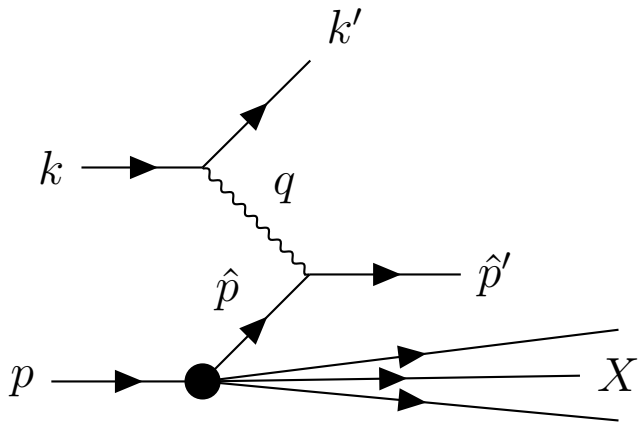

Figure 2. Feynman diagram of deep inelastic scattering in the parton model. Incident lepton has four-momentum k and energy E, the nucleon p and E_p, the struck quark $\hat{p}$ and $\hat{E}$. Lepton and quark interact via a virtual particle with four-momentum q, resulting in outgoing lepton with k' and energy E' and the proton remnants X, including the quark $\hat{p}'$.

2.2 Parton level cross section

In the parton model, the proton is considered to consist of point-like particles, partons. These particles are quarks, antiquarks and gluons. In the lowest order (LO) in perturbative quantum chromodynamics (pQCD), the only contributing processes in DIS are electroweak interactions with photon, Z^0 or $W^\pm$ exchange. Since the electron doesn't experience strong interaction directly, it scatters off a quark or an antiquark. The gluon-initiated scattering can take place only in higher orders in pQCD. Here we only consider LO scattering where the struck parton is a quark. The antiquark contributions are included in the final form of the cross section, but not explicitly considered in the calculation. In this notation, the 4-vectors p_a, p_b, p_c are k, p, k' and energies E_c to E' and so on. The incoming parton has momentum $\hat{p} = \xi p$, where ξ is the fraction of proton's momentum carried by the quark. Some useful Lorentz-invariant quantities are

$$\begin{aligned} x &= \frac{-q^2}{2(p \cdot q)} \text{ Bjorken } x\text{, equal to } \xi \text{ in the parton model,} \\ Q^2 &= -q^2 = (k - k')^2 \text{ propagator virtuality,} \\ y &= \frac{q \cdot p}{k \cdot p} \text{ inelasticity, the lepton energy loss fraction in proton rest frame,} \\ W^2 &= (p + q)^2 \text{ invariant mass of the hadronic system } X. \end{aligned} \tag{8}$$

The three-momenta $|\vec{p}|$ is given by the dispersion relation

$$|\vec{p}| = \sqrt{E^2 - m^2}. \tag{9}$$

The parton level cross section for a lepton scattering off a quark is given by equation (7) as

$$d\hat{\sigma}(l + q \to l + q) = \frac{\overline{|\mathcal{M}|^2}}{4(k \cdot \hat{p})}(2\pi)^4 \delta^{(4)}(k + \hat{p} - k' - \hat{p}') \frac{d^3k'}{2E'(2\pi)^3} \frac{d^3\hat{p}'}{2\hat{E}'(2\pi)^3} \tag{10}$$

The delta function can be partly integrated out by inserting a unit operator in the following form:

$$\mathbb{1} = \int d\hat{E} 2\hat{E}' \theta(\hat{E}') \underbrace{\delta(|\hat{p}'|^2)}_{\delta(g(\hat{E}'))}, \tag{11}$$

$$\text{where } \delta(g(x)) = \sum_i \frac{\delta(x - x_i)}{|g'(x_i)|} \Rightarrow \delta(g(\hat{E}')) = \sum_i \frac{\delta(\hat{E}' - \hat{E}'_i)}{|2\hat{E}'_i|}. \tag{12}$$

Here the roots of g are $g(\hat{E}'_i) = (\hat{E}')^2 - |\vec{\hat{p}}'|^2 = 0 \Leftrightarrow \hat{E}'_i = \pm|\vec{\hat{p}}'|$, and the step function $\theta(\hat{E}')$ ensures we pick only the positive value in the integrand. The integral is then

$$\int d\hat{E}' \frac{2\hat{E}'}{2|\vec{\hat{p}}'|} \delta(\hat{E}' - |\vec{\hat{p}}'|) = \mathbb{1}$$

and so the differential phase space element can be made into a 4-dimensional integral, reducing the dimension of the delta function

$$\underbrace{\mathbb{1}}_{\downarrow} = \int d\hat{E}' 2\hat{E}' \theta(\hat{E}') \delta(|\hat{p}'|^2)$$

$$\int \frac{d^3\vec{\hat{p}}'}{2\hat{E}'} \delta^{(4)}(q + \hat{p} - \hat{p}') = \int d^4\hat{p}' \theta(\hat{E}') \delta(|\hat{p}'|^2) \delta^{(4)}(q + \hat{p} - \hat{p}')$$

$$= \delta((q + \hat{p})^2) = \delta(\underbrace{q^2}_{=-Q^2} + \cancelto{0}{\hat{p}^2} + 2(q \cdot \hat{p}))$$

$$= \delta(-x2(p \cdot q) + \xi 2(p \cdot q)) = \frac{1}{2(p \cdot q)} \delta(\xi - x)$$

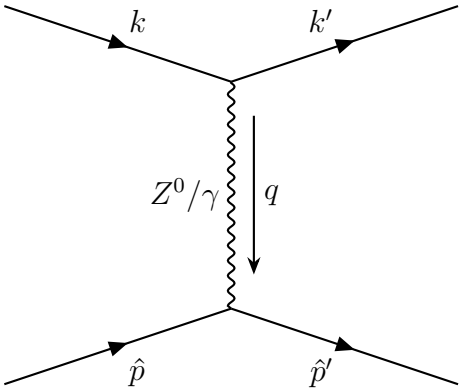

Figure 3. Electron and quark interaction via exchanged photon γ or Z boson.

resulting in

$$d\hat{\sigma} = \frac{\overline{|\mathcal{M}|^2}}{8(k\cdot\hat{p})(p\cdot q)}\frac{d^3k'}{(2\pi)^2 2E'}\delta(\xi - x) = \frac{\overline{|\mathcal{M}|^2}}{64\pi^2}\frac{d^3k'}{E'\xi(k\cdot p)(p\cdot q)}\delta(\xi - x). \tag{13}$$

Using spherical coordinates $d^3\vec{k}' = |\vec{k}'|^2 d|\vec{k}'|d\Omega = E'^2 dE' d\Omega$ leads to parton level cross section for lepton scattering of a single quark flavor

$$\frac{d^2\hat{\sigma}}{dE'd\Omega} = \frac{\overline{|\mathcal{M}|^2}}{64\pi^2}\frac{E'}{\xi(k\cdot p)(p\cdot q)}\delta(\xi - x). \tag{14}$$

2.3 Parton level invariant amplitude $\overline{|\mathcal{M}|^2}$

The invariant amplitude can be calculated using Feynman rules from appendix A for the leading order graph 3. The neutral-current invariant amplitude takes into account both photon and Z boson interaction,

$$|\mathcal{M}|^2 = |\mathcal{M}^\gamma + \mathcal{M}^Z|^2 = |\mathcal{M}^\gamma|^2 + |\mathcal{M}^Z|^2 + 2\mathrm{Re}(\mathcal{M}^{\gamma\dagger}\mathcal{M}^Z),$$

which leads to an interference term as well. The amplitude for the photon exchange is

$$-i\mathcal{M}^\gamma = \bar{u}(k',s')iQ_e e\gamma^\mu u(k,s)\frac{ig_{\mu\nu}}{q^2}\bar{u}(\hat{p}',r')iQ_q e\gamma^\nu u(\hat{p},r) \tag{15}$$

$$|\mathcal{M}^\gamma|^2 = \mathcal{M}^{\gamma\dagger}\mathcal{M}^\gamma = \left(\frac{iQ_eQ_qe^2}{q^2}\bar{u}_{k'}\gamma^\mu u_k g_{\mu\nu}\bar{u}_{\hat{p}'}\gamma^\nu u_{\hat{p}}\right)^\dagger \times \frac{iQ_eQ_qe^2}{q^2}\bar{u}_{k'}\gamma^\mu u_k g_{\mu\nu}\bar{u}_{\hat{p}'}\gamma^\nu u_{\hat{p}}.$$

Taking the conjugate transpose, raising and lowering indices, reordering the spinors, averaging over initial states and summing over final states gives the averaged amplitude squared

$$\overline{|\mathcal{M}^\gamma|^2} = \frac{1}{2}\sum_r \frac{1}{2}\sum_s \sum_{r'}\sum_{s'} |\mathcal{M}^\gamma|^2 = \frac{e^4}{q^4}\underbrace{\frac{1}{2}\sum_{s,s'} u_k \bar{u}_k \gamma^\mu u_{k'} \bar{u}_{k'} \gamma^\nu}_{L_\gamma^{\mu\nu}} \underbrace{\frac{1}{2} Q_q^2 \sum_{r,r'} u_{\hat{p}} \bar{u}_{\hat{p}} \gamma_\mu u_{\hat{p}'} \bar{u}_{\hat{p}'} \gamma_\nu}_{Q^\gamma_{\mu\nu}}. \tag{16}$$

The defined leptonic tensor $L_\gamma^{\mu\nu}$ and quark tensor $Q^\gamma_{\mu\nu}$ can be calculated using projection operators

$$\sum_s u(p,s)\bar{u}(p,s) = (\not{p} + \cancel{m}) \overset{\approx 0}{=} p_\mu \gamma^\mu = p^\mu \gamma_\mu \tag{17}$$

and traces

$$\mathrm{TR}(\gamma_a \gamma_b \gamma_c \gamma_d) = 4[g_{ab}g_{cd} - g_{ac}g_{bd} + g_{ad}g_{cb}], \tag{18}$$

since the Lorentz-indices (i, j, k...) go around after the re-ordering:

$$\begin{aligned} L_\gamma^{\mu\nu} &= \frac{1}{2}\sum_{s,s'} u_{k(l)} \bar{u}_{k(i)} \gamma^\mu_{(ij)} u_{k'(j)} \bar{u}_{k'(k)} \gamma^\nu_{(kl)} = \frac{1}{2} \not{k}_{(li)} \gamma^\mu_{(ij)} \not{k}'_{(jk)} \gamma^\nu_{(kl)} \\ &= \frac{1}{2} k_\alpha k'_\beta \mathrm{TR}(\gamma^\alpha \gamma^\mu \gamma^\beta \gamma^\nu) \\ &= 2[k'^\mu k^\nu + k'^\nu k^\mu - (k \cdot k') g^{\mu\nu}] \qquad (19) \\ Q^\gamma_{\mu\nu} &= 2Q_q^2[\hat{p}'_\mu \hat{p}_\nu + \hat{p}'_\nu \hat{p}_\mu - (\hat{p} \cdot \hat{p}') g_{\mu\nu}] \qquad (20) \\ \overline{|\mathcal{M}^\gamma|^2} &= \frac{e^4}{q^4} L_\gamma^{\mu\nu} Q^\gamma_{\mu\nu}. \qquad (21) \end{aligned}$$

The amplitude for Z boson exchange, figure 3, can be written with appendix A Feynman rules as

$$\begin{aligned} -i\mathcal{M}_Z &= \bar{u}(k',s') i g_Z \gamma^\mu \Big[L_f(1-\gamma^5) + R_f(1+\gamma^5) \Big] u(k,s) \\ \times &\Big[\frac{i g_{\mu\nu}}{q^2 - M_Z^2} - \frac{i q_\mu q_\nu}{M_Z^2 (q^2 - M_Z^2)} \Big] \bar{u}(\hat{p}',r') i g_Z \gamma^\nu \Big[L_f(1-\gamma^5) + R_f(1+\gamma^5) \Big] u(\hat{p},r). \end{aligned} \tag{22}$$

This can already be simplified. The $q_\mu q_\nu$ term in the propagator cancels with the spinors u and anti-spinors $\bar{u}$ after using Dirac equation (neglecting lepton masses)

$$(\not{p} - m)u(p,s) = 0 \qquad \bar{u}(p,s)(\not{p} - m) = 0 \tag{23}$$

and moving the gamma matrices to form $\not{k}$ using their anti-commutativity $\{\gamma^\mu, \gamma^5\} = 0$

$$\begin{aligned}
&\bar{u}_{k'}\gamma^\mu[L_f(1-\gamma^5) + R_f(1+\gamma^5)]u_k q_\mu \\
=&\bar{u}_{k'}(\not{k} - \not{k}')[L_f(1-\gamma^5) + R_f(1+\gamma^5)]u_k \\
=&\bar{u}_{k'}[L_f(1+\gamma^5) + R_f(1-\gamma^5)]\not{k}u_k - \bar{u}_{k'}\not{k}'[L_f(1+\gamma^5) + R_f(1-\gamma^5)]u_k = 0.
\end{aligned}$$

Squaring the amplitude, summing and averaging over states and using the metric $g_{\mu\nu}$ to lower one index gives

$$\begin{aligned}
\overline{|\mathcal{M}_Z|^2} =& \frac{1}{2}\sum_r \frac{1}{2}\sum_s \sum_{r'}\sum_{s'} |\mathcal{M}_Z|^2 = \frac{g_Z^4}{(q^2 - M_Z^2)^2} \\
&\underbrace{\frac{1}{2}\sum_{s,s'} u_k \bar{u}_k \gamma^\mu [L_e(1-\gamma^5) + R_e(1+\gamma^5)] u_{k'} \bar{u}_{k'} \gamma^\nu [L_e(1-\gamma^5) + R_e(1+\gamma^5)]}_{L_Z^{\mu\nu}} \\
&\underbrace{\frac{1}{2}\sum_{r,r'} u_{\hat{p}} \bar{u}_{\hat{p}} \gamma_\mu [L_q(1-\gamma^5) + R_q(1+\gamma^5)] u_{\hat{p}'} \bar{u}_{\hat{p}'} \gamma_\nu [L_q(1-\gamma^5) + R_q(1+\gamma^5)]}_{Q_{\mu\nu}^Z}.
\end{aligned}$$

The traces can be calculated similarly as before, but now using $(\gamma^5)^2 = 1$ and $\mathrm{TR}(\gamma^\alpha\gamma^\mu\gamma^\beta\gamma^\nu\gamma^5) = -4i\epsilon^{\alpha\mu\beta\nu}$ as well

$$\begin{aligned}
L_Z^{\mu\nu} &= \frac{1}{2}\not{k}\gamma^\mu[L_e(1-\gamma^5) + R_e(1+\gamma^5)]\not{k}'\gamma^\nu[L_e(1-\gamma^5) + R_e(1+\gamma^5)] \\
&= \frac{1}{2}\{L_e^2\mathrm{TR}[\not{k}\gamma^\mu(1-\gamma^5)\not{k}'\gamma^\nu(1-\gamma^5)] \\
&+ L_eR_e\mathrm{TR}[\not{k}\gamma^\mu(1-\gamma^5)\not{k}'\gamma^\nu(1+\gamma^5)] \\
&+ R_eL_e\mathrm{TR}[\not{k}\gamma^\mu(1+\gamma^5)\not{k}'\gamma^\nu(1-\gamma^5)] \\
&+ R_e^2\mathrm{TR}[\not{k}\gamma^\mu(1+\gamma^5)\not{k}'\gamma^\nu(1+\gamma^5)]\} \\
&= 4L_e^2[k^\mu k'^\nu + k^\nu k'^\mu - (k\cdot k')g^{\mu\nu} + i\epsilon^{\alpha\mu\beta\nu}k_\alpha k'_\beta] \\
&+ 4R_e^2[k^\mu k'^\nu + k^\nu k'^\mu - (k\cdot k')g^{\mu\nu} - i\epsilon^{\alpha\mu\beta\nu}k_\alpha k'_\beta] \\
L_Z^{\mu\nu} &= 4(L_e^2+R_e^2)[k^\mu k'^\nu + k^\nu k'^\mu - (k\cdot k')g^{\mu\nu}] + 4(L_e^2-R_e^2)i\epsilon^{\alpha\mu\beta\nu}k_\alpha k'_\beta \\
Q_{\mu\nu}^Z &= 4(L_q^2+R_q^2)[\hat{p}_\mu\hat{p}'_\nu + \hat{p}_\nu\hat{p}'_\mu - (\hat{p}\cdot\hat{p}')g_{\mu\nu}] + 4(L_q^2-R_q^2)i\epsilon_{\alpha\mu\beta\nu}\hat{p}^\alpha\hat{p}'^\beta.
\end{aligned}$$

For the interference term we get

$$\begin{aligned}
\overline{\mathcal{M}_\gamma^\dagger\mathcal{M}_Z} &= -\frac{e^2g_Z^2}{q^2(q^2-M_Z^2)}L_{\gamma Z}^{\mu\nu}Q_{\mu\nu}^{\gamma Z} \\
L_{\gamma Z}^{\mu\nu} &= 2(L_e+R_e)[k^\mu k'^\nu + k^\nu k'^\mu - (k\cdot k')g^{\mu\nu}] + 2(L_e-R_e)i\epsilon^{\alpha\mu\beta\nu}k_\alpha k'_\beta \\
Q_{\mu\nu}^{\gamma Z} &= 2Q_q(L_q+R_q)[\hat{p}'_\mu\hat{p}_\nu + \hat{p}'_\nu\hat{p}_\mu - (\hat{p}\cdot\hat{p}')g_{\mu\nu}] + 2Q_q(L_q-R_q)i\epsilon_{\alpha\mu\beta\nu}\hat{p}^\alpha\hat{p}'^\beta.
\end{aligned}$$

The full amplitude is then

$$\begin{aligned}
\overline{|\mathcal{M}|^2} &= \overline{|\mathcal{M}_\gamma|^2} + \overline{|\mathcal{M}_Z|^2} + 2\mathrm{Re}(\overline{\mathcal{M}_\gamma^\dagger\mathcal{M}_Z}) &(24)\\
&= \frac{e^4}{q^4}L_\gamma^{\mu\nu}Q_{\mu\nu}^\gamma + \frac{g_Z^4}{(q^2-M_Z^2)^2}L_Z^{\mu\nu}Q_{\mu\nu}^Z - \frac{2e^2g_Z^2}{q^2(q^2-M_Z^2)}(L_{\gamma Z}^{\mu\nu}Q_{\mu\nu}^{\gamma Z}). &(25)
\end{aligned}$$

After substituting this into equation (14) and multiplying by E/E the parton level cross section for one quark flavor is

$$\frac{d^2\hat{\sigma}}{dE'd\Omega} = \frac{\overline{|\mathcal{M}|^2}}{64\pi^2}\frac{E'}{\xi(k\cdot p)(p\cdot q)}\delta(\xi-x) = \frac{E'}{16\pi^2E}\frac{E\delta(\xi-x)}{4\xi(k\cdot p)(p\cdot q)}\overline{|\mathcal{M}|^2}. \qquad (26)$$

2.4 DIS with proton target

Deriving the full cross section with no prior knowledge of the proton's structure leads to unknown hadronic tensors. The parton model cross section enables the identification of these hadronic tensors and the structure functions. In this calculation there are no assumptions made about the structure of the proton. The contribution of the proton in the interactions is given by a hadronic matrix element

$$\langle X(p_X,\sigma_X)|\Lambda J^\nu|h(p,\sigma)\rangle\,, \tag{27}$$

where J^ν is the hadronic part of the operator between initial state $h(p,\sigma)$ and final state X, and Λ is the vertex factor of the interaction.

Considering both photon and Z boson interaction in the scattering process shown in figure 1 gives invariant amplitude

$$\begin{aligned}
-i\mathcal{M} &= -i\mathcal{M}_\gamma - i\mathcal{M}_Z \\
&= \bar{u}_{k'} iQ_e e\gamma^\mu u_k \left[\frac{ig_{\mu\nu}}{q^2}\right] \langle X|iQ_p eJ^\nu_\gamma|h\rangle + \bar{u}_{k'} g_z\gamma^\mu[L_e(1-\gamma^5) \\
&+ R_e(1+\gamma^5)]u_k\left[\frac{-ig_{\mu\nu}}{q^2-M_Z^2} + \frac{q_\mu q_\nu}{M_Z^2(q^2-M^2)}\right]\langle X|ig_z J^\nu_Z|h\rangle \\
&= \frac{-ie^2}{q^2}\bar{u}_{k'}\gamma^\mu u_k \langle X|eJ^\gamma_\mu|h\rangle + \frac{ig_z^2}{q^2-M_Z^2}\bar{u}_{k'}\gamma^\mu \underbrace{[L_e(1-\gamma^5)+R_e(1+\gamma^5)]}_{\mathcal{V}} u_k \langle X|J^Z_\mu|h\rangle\,,
\end{aligned}$$

which is then squared and sum-averaged. A shorthand $\mathcal{V}$ is used for the fermion-Z boson vertex factor.

$$\begin{aligned}
\overline{|\mathcal{M}|^2} &= \overline{|\mathcal{M}_\gamma|^2} + \overline{|\mathcal{M}_Z|^2} + 2\mathrm{Re}(\overline{|\mathcal{M}^\dagger_\gamma \mathcal{M}_Z|}) \\
&= \frac{e^4}{q^4}\underbrace{\frac{1}{2}\sum_{s,s'}\bar{u}_k\gamma^\mu u_{k'}\bar{u}_{k'}\gamma^\nu u_k}_{L^{\mu\nu}_\gamma}\frac{1}{2}\sum_{\sigma,\sigma_X}\langle h|J^{\gamma\dagger}_\mu|X\rangle\langle X|J^\gamma_\nu|h\rangle \\
&+ \frac{g_Z^4}{(q^2-M_Z^2)^2}\underbrace{\frac{1}{2}\sum_{s,s'}\bar{u}_k\gamma^\mu\mathcal{V}u_{k'}\bar{u}_{k'}\gamma^\nu\mathcal{V}u_k}_{L^{\mu\nu}_Z}\frac{1}{2}\sum_{\sigma,\sigma_X}\langle h|J^{Z\dagger}_\mu|X\rangle\langle X|J^Z_\nu|h\rangle \\
&+ 2\mathrm{Re}\Big(\frac{-e^2}{q^2}\frac{g_Z^2}{(q^2-M_Z^2)}\underbrace{\frac{1}{2}\sum_{s,s'}\bar{u}_k\gamma^\mu u_{k'}\bar{u}_{k'}\gamma^\nu\mathcal{V}u_k}_{L^{\mu\nu}_{\gamma Z}}\frac{1}{2}\sum_{\sigma,\sigma_X}\langle h|J^{\gamma\dagger}_\mu|X\rangle\langle X|J^Z_\nu|h\rangle\Big).
\end{aligned}$$

The leptonic tensors are defined similarly as above, and in order to define the hadronic tensors the cross section (3) is needed

$$\begin{aligned} d\sigma =& \frac{\overline{|\mathcal{M}|^2}}{4(k\cdot p)}(2\pi)^4\delta^{(4)}(k+p-k'-\sum_{j=1}^{n}p_j)\frac{d^3\vec{k'}}{2E'(2\pi)^3}\prod_{i=1}^{n}\frac{d^3\vec{p_i}}{2E_i(2\pi)^3} \\ =& \frac{4\pi M}{4(p\cdot k)}\frac{d^3\vec{k'}}{2E'(2\pi)^3}\Big[\frac{e^4}{q^4}L_\gamma^{\mu\nu}W_{\mu\nu}^\gamma + \frac{g_Z^4}{(q^2-M_Z^2)^2}L_Z^{\mu\nu}W_{\mu\nu}^Z \\ & -\frac{2e^2g_Z^2}{q^2(q^2-M_Z^2)}\mathrm{Re}(L_{\gamma Z}^{\mu\nu}W_{\mu\nu}^{\gamma Z})\Big]. \end{aligned}$$

Here the hadronic tensors are defined by absorbing the delta-function, π factors, product of phase-space differentials and the conventional factor of $1/4\pi M$ with the braket terms

$$\underbrace{\frac{1}{4\pi M}(2\pi)^4\delta^{(4)}(k+p-k'-\sum_{j=1}^{n}p_j)\prod_{i=1}^{n}\frac{d^3\vec{p_i}}{2E_i(2\pi)^3}\frac{1}{2}\sum_{\sigma,\sigma_X}\langle h|J_\mu^\dagger|X\rangle\langle X|J_\nu|h\rangle}_{\text{Define hadronic tensors } W_{\mu\nu}}. \tag{28}$$

Using spherical coordinates to get the differentials in target rest frame

$$(p\cdot k) = ME, \qquad d^3\vec{k'} = E'^2dE'd\Omega,$$

the differential cross section is then formed as

$$\frac{d^2\sigma}{dE'd\Omega} = \frac{E'}{16\pi^2E}\Big[\frac{e^4}{q^4}L_\gamma^{\mu\nu}W_{\mu\nu}^\gamma + \frac{g_Z^4}{(q^2-M_Z^2)^2}L_Z^{\mu\nu}W_{\mu\nu}^Z - \frac{2e^2g_Z^2}{q^2(q^2-M_Z^2)}(L_{\gamma Z}^{\mu\nu}W_{\mu\nu}^{\gamma Z})\Big]. \tag{29}$$

Taking the parton level cross section and summing over quark flavors and integrating over momentum fraction distributions ξ the full cross section

$$d\sigma = \sum_q \int d\xi q(\xi)d\hat{\sigma} \tag{30}$$

where the universal, process-independent parton distribution function $q(\xi)$ is introduced. It gives the probability of finding a parton q with momentum fraction

ξ.

$$\begin{aligned}\frac{d^2\sigma}{dE'd\Omega} = \frac{E'}{16\pi^2 E}\Big[&\frac{e^4}{q^4}L_\gamma^{\mu\nu}\sum_q\int d\xi q(\xi)\frac{E\delta(\xi-x)}{4\xi(k\cdot p)(p\cdot q)}Q_{\mu\nu}^\gamma \\ &+\frac{g_Z^4}{(q^2-M_Z^2)}L_Z^{\mu\nu}\sum_q\int d\xi q(\xi)\frac{E\delta(\xi-x)}{4\xi(k\cdot p)(p\cdot q)}Q_{\mu\nu}^Z \\ &-\frac{2e^2g_Z^2}{q^2(q^2-M_Z^2)}L_{\gamma Z}^{\mu\nu}\sum_q\int d\xi q(\xi)\frac{E\delta(\xi-x)}{4\xi(k\cdot p)(p\cdot q)}Q_{\mu\nu}^{\gamma Z}\Big]. \qquad (31)\end{aligned}$$

The form of the hadronic tensors can be identified by comparing equations (29) and (31).

2.5 Structure functions

The DIS cross sections are often given in terms of structure functions. These describe the structure of the target hadron relevant for a given scattering. The proton structure functions can be read by first writing the hadronic and quark tensors in a general Lorentz-structure form.

2.5.1 Hadronic tensor Lorentz-structure

The hadronic tensor has a Lorentz-structure which can depend only on p_μ and q_μ. It can thus be written in a general form using four-vectors with unknown coefficients A_i as

$$\begin{aligned}W_{\mu\nu} &= A_1 g_{\mu\nu} + A_2 p_\mu p_\nu + A_3(p_\mu q_\nu + p_\nu q_\mu) + A_5 q_\mu q_\nu && (32)\\ &+ A_4(p_\mu q_\nu - p_\nu q_\mu) + iA_6\epsilon_{\mu\nu\gamma\delta}p^\gamma q^\delta && (33)\\ &= W_{\mu\nu}^S + W_{\mu\nu}^A. && (34)\end{aligned}$$

The symmetric part $W_{\mu\nu}^S$ consists of A_1, A_2 and A_3. Contracting symmetric and anti-symmetric tensors gives zero. The number of coefficients can be reduced using the continuity equation

$$q^\mu W_{\mu\nu}^S = 0 \quad = \quad A_1 q_\nu + A_2(q\cdot p)p_\nu + A_3[(q\cdot p)q_\nu + q^2 p_\nu] + A_5 q^2 q_\nu \qquad (35)$$

which leads to a pair of equations for linearly independent p_ν and q_ν

$$\begin{cases} (A_1 + A_3(q\cdot p) + A_5 q^2)q_\nu &= 0, \qquad A_5 = -\frac{A_1}{q^2} + \frac{(p\cdot q)^2}{q^4}A_2 \\ (A_2(q\cdot p) + A_3 q^2)p_\nu &= 0, \qquad A_3 = -\frac{(q\cdot p)}{q^2}A_2 \end{cases}. \tag{36}$$

This makes the symmetric part of hadronic tensor

$$W^S_{\mu\nu} = A_1(g_{\mu\nu} - \frac{q_\mu q_\nu}{q^2}) + A_2(p_\mu - \frac{(q\cdot p)}{q^2}q_\mu)(p_\nu - \frac{(q\cdot p)}{q^2}q_\nu). \tag{37}$$

Further defining structure factors $W_1 = -A_1$ and $W_2 = A_2 M^2$ leads to

$$W^S_{\mu\nu} = -W_1(g_{\mu\nu} - \frac{q_\mu q_\nu}{q^2}) + \frac{W_2}{M^2}(p_\mu - \frac{(q\cdot p)}{q^2}q_\mu)(p_\nu - \frac{(q\cdot p)}{q^2}q_\nu). \tag{38}$$

The leptonic tensors may have antisymmetric parts as well. Using the continuity equation for the antisymmetric part yields

$$q^\mu W^A_{\mu\nu} = q^\mu A_4(p_\mu q_\nu - p_\nu q_\mu) + q^\mu i A_6 \epsilon_{\mu\nu\alpha\beta}p^\alpha q^\beta \tag{39}$$

$$= A_4[(p\cdot q) - q^2 p_\nu] + iA_6 q^\mu \epsilon_{\mu\nu\alpha\beta}p^\alpha q^\beta = 0. \tag{40}$$

This equation must also hold for linearly independent q_ν and p_ν as

$$\begin{cases} A_4(q\cdot p)q_\nu + A_6 q^\mu \epsilon_{\mu\nu\alpha\beta}p^\alpha q^\beta &= 0 \\ A_4 q^2 p_\nu + A_6 q^\mu \epsilon_{\mu\nu\alpha\beta}p^\alpha q^\beta &= 0 \end{cases}. \tag{41}$$

The Levi-Civita symbol ϵ is antisymmetric in exchange of two indices. By swapping the indices μ and β we get $q^\mu \epsilon_{\mu\nu\alpha\beta}p^\alpha q^\beta = -q^\beta \epsilon_{\beta\nu\alpha\mu}p^\alpha q^\mu = 0$. This means that the pair of equations is only satisfied if $A_4 = 0$. The antisymmetric part of $W_{\mu\nu}$ is then

$$W^A_{\mu\nu} = iA_6 \epsilon_{\mu\nu\alpha\beta}p^\alpha q^\beta. \tag{42}$$

Defining the structure factor $W_3 = -2M^2 A_6$ gives the full hadronic tensor as

$$W_{\mu\nu} = -W_1(g_{\mu\nu} - \frac{q_\mu q_\nu}{q^2}) + \frac{W_2}{M^2}(p_\mu - \frac{(q\cdot p)}{q^2}q_\mu)(p_\nu - \frac{(q\cdot p)}{q^2}q_\nu) - \frac{W_3}{2M^2}i\epsilon_{\mu\nu\alpha\beta}p^\alpha q^\beta. \tag{43}$$

2.5.2 Quark tensor Lorentz-structure

The quark tensor $Q^{\gamma}_{\mu\nu} = Q_q^2 2[\hat{p}'_\mu \hat{p}_\nu + \hat{p}'_\nu \hat{p}_\mu - (\hat{p}\cdot\hat{p}')g_{\mu\nu}]$ can be modified to resemble the general form of the hadronic tensor (38) by suitably adding and multiplying by

$$\frac{q_\mu q_\nu}{q^2}(\hat{p}\cdot q) - \frac{q_\mu q_\nu}{q^2}(\hat{p}\cdot q) = 0 \qquad (\bullet)$$

$$\frac{-2\xi(p\cdot q)}{q^2} = 1, \text{ since } q^2 = (\hat{p}'-\hat{p})^2 = -2(\hat{p}\cdot\hat{p}') = -2(\hat{p}\cdot(\hat{p}+q)) = -2(\hat{p}\cdot q) \quad (*)$$

and using $\hat{p} = \xi p$, $\hat{p}' = q + \hat{p}$ in the following way

$$\begin{aligned}
&\hat{p}'_\mu \hat{p}_\nu + \hat{p}'_\nu \hat{p}_\mu \underbrace{\uparrow}_{(\bullet)} - \underbrace{(\hat{p}\cdot\hat{p}')g_{\mu\nu}}_{(\hat{p}\cdot q)g_{\mu\nu}} \\
=&\hat{p}_\mu \hat{p}_\nu + q_\mu \hat{p}_\nu \underbrace{\uparrow}_{(*)} + \hat{p}_\nu \hat{p}_\mu + q_\nu \hat{p}_\mu \underbrace{\uparrow}_{(*)} + \frac{q_\mu q_\nu}{q^2}(\hat{p}\cdot q) - \frac{q_\mu q_\nu}{q^2}(\hat{p}\cdot q)\underbrace{\uparrow}_{(*)} - (\hat{p}\cdot q)g_{\mu\nu} \\
=&2\xi^2\Big(p_\mu p_\nu - \frac{(p\cdot q)}{q^2}(q_\mu p_\nu + q_\nu p_\mu) + \frac{(p\cdot q)^2}{q^4}\Big) - \xi(p\cdot q)\Big(g_{\mu\nu} - \frac{q_\mu q_\nu}{q^2}\Big) \\
=&-\xi(p\cdot q)\Big(g_{\mu\nu} - \frac{q_\mu q_\nu}{q^2}\Big) + 2\xi^2\Big(p_\mu - \frac{(q\cdot p)}{q^2}q_\mu\Big)\Big(p_\nu - \frac{(q\cdot p)}{q^2}q_\nu\Big).
\end{aligned}$$

Now we can compare the equations of the parton-model differential cross section (31) and the leading order differential cross section of a hadron target (29) and see the hadronic tensor and the terms of the quark tensor $Q^{\gamma}_{\mu\nu}$

$$\begin{aligned}
Q^{\gamma}_{\mu\nu} &= Q_q^2\Big[-2\xi(p\cdot q)\Big(g_{\mu\nu} - \frac{q_\mu q_\nu}{q^2}\Big) + 4\xi^2\Big(p_\mu - \frac{(q\cdot p)}{q^2}q_\mu\Big)\Big(p_\nu - \frac{(q\cdot p)}{q^2}q_\nu\Big)\Big] \\
W^{\gamma}_{\mu\nu} &= \sum_q \int d\xi q(\xi)\frac{E\delta(\xi - x)}{4\xi(k\cdot p)(q\cdot p)}Q_q^2\Big[-2\xi(p\cdot q)\Big(g_{\mu\nu} - \frac{q_\mu q_\nu}{q^2}\Big) \\
&\quad + 4\xi^2\Big(p_\mu - \frac{(q\cdot p)}{q^2}q_\mu\Big)\Big(p_\nu - \frac{(q\cdot p)}{q^2}q_\nu\Big)\Big] \\
&= \underbrace{-\sum_q q(x)\frac{Q_q^2}{2M}}_{-W_1^\gamma}\Big(g_{\mu\nu} - \frac{q_\mu q_\nu}{q^2}\Big) + \underbrace{\sum_q x\frac{Q_q^2}{M(p\cdot q)}q(x)}_{\frac{W_2^\gamma}{M^2}}\Big(p_\mu - \frac{(q\cdot p)}{q^2}q_\mu\Big)\Big(p_\nu - \frac{(q\cdot p)}{q^2}q_\nu\Big) \\
&= -W_1^\gamma\Big(g_{\mu\nu} - \frac{q_\mu q_\nu}{q^2}\Big) + \frac{W_2^\gamma}{M^2}\Big(p_\mu - \frac{(q\cdot p)}{q^2}q_\mu\Big)\Big(p_\nu - \frac{(q\cdot p)}{q^2}q_\nu\Big).
\end{aligned}$$

For the whole electroweak interaction the anti-symmetric part has to be modified as well. The epsilon-term can be written as

$$i\epsilon_{\alpha\mu\beta\nu}\hat{p}^\alpha\hat{p}'^\beta = i\epsilon_{\alpha\mu\beta\nu}p^\alpha\xi(\hat{p}^\beta + q^\beta) = i\xi(\xi \underbrace{p^\alpha p^\beta\epsilon_{\alpha\mu\beta\nu}}_{\text{sym}\,\times\,\text{antisym}\,=0} + p^\alpha q^\beta\epsilon_{\alpha\mu\beta\nu}) = i\xi p^\alpha q^\beta\epsilon_{\alpha\mu\beta\nu}. \tag{44}$$

Looking at the quark tensors term by term and modifying as

$$\begin{aligned}
Q^\gamma_{\mu\nu} &= Q_q^2 2[\hat{p}'_\mu\hat{p}_\nu + \hat{p}'_\nu\hat{p}_\mu - (\hat{p}\cdot\hat{p}')g_{\mu\nu}] \\
Q^Z_{\mu\nu} &= 2(L_q^2+R_q^2)2[\hat{p}'_\mu\hat{p}_\nu + \hat{p}'_\nu\hat{p}_\mu - (\hat{p}\cdot\hat{p}')g_{\mu\nu}] + 4(L_q^2-R_q^2)i\epsilon_{\alpha\mu\beta\nu}p^\alpha p'^\beta \\
&= \frac{2(L_q^2+R_q^2)}{Q_q^2}Q^\gamma_{\mu\nu} + 4(L_q^2-R_q^2)\xi i\epsilon_{\alpha\mu\beta\nu}p^\alpha q^\beta \\
Q^{\gamma Z}_{\mu\nu} &= Q_q(L_q+R_q)2[\hat{p}'_\mu\hat{p}_\nu + \hat{p}'_\nu\hat{p}_\mu - (\hat{p}\cdot\hat{p}')g_{\mu\nu}] + 2Q_q(L_q-R_q)i\epsilon_{\alpha\mu\beta\nu}p^\alpha p'^\beta \\
&= \frac{(L_q+R_q)}{Q_q}Q^\gamma_{\mu\nu} + 2(L_q-R_q)\xi i\epsilon_{\alpha\mu\beta\nu}p^\alpha q^\beta
\end{aligned}$$

gives a simple form to acquire the structure functions, as was done for pure photon interaction. The Z term can be compared to the general Lorentz structure of the hadronic tensor (43) after integration over momentum distribution,

$$\begin{aligned}
W^Z_{\mu\nu} &= \sum_q\int d\xi q(\xi)\frac{E\delta(\xi-x)}{4\xi(k\cdot p)(p\cdot q)}\Big[2(L_q^2+R_q^2)\frac{Q^\gamma_{\mu\nu}}{Q_q^2} + 4(L_q^2-R_q^2)\xi i\epsilon_{\alpha\mu\beta\nu}p^\alpha q^\beta\Big] \\
&= \sum_q\int d\xi q(\xi)\frac{E\delta(\xi-x)}{4\xi(k\cdot p)(p\cdot q)}\Big\{2(L_q^2+R_q^2)\Big[-2\xi(p\cdot q)\Big(g_{\mu\nu}-\frac{q_\mu q_\nu}{q^2}\Big)+ \\
&\quad 4\xi^2\Big(p_\mu-\frac{(p\cdot q)}{q^2}q_\mu\Big)\Big(p_\nu-\frac{(p\cdot q)}{q^2}q_\nu\Big)\Big] + 4(L_q^2-R_q^2)\xi i\epsilon_{\alpha\mu\beta\nu}p^\alpha q^\beta\Big\} \\
&= \underbrace{-\sum_q\frac{(L_q^2+R_q^2)}{M}q(x)}_{-W_1^Z}\Big(g_{\mu\nu}-\frac{q_\mu q_\nu}{q^2}\Big) \\
&\quad + \underbrace{\sum_q\frac{2x(L_q^2+R_q^2)}{M(p\cdot q)}q(x)}_{\frac{W_2^Z}{M^2}}\Big(p_\mu-\frac{(p\cdot q)}{q^2}q_\mu\Big)\Big(p_\nu-\frac{(p\cdot q)}{q^2}q_\nu\Big) \\
&\quad + \underbrace{\sum_q\frac{(L_q^2-R_q^2)}{M(p\cdot q)}q(x)}_{\frac{W_3^Z}{2M^2}}i\epsilon_{\alpha\mu\beta\nu}p^\alpha q^\beta.
\end{aligned}$$

It can be seen that the first two structure functions differ from W_1^γ and W_2^γ only by a factor of $2(L_q^2+R_q^2)/Q_q^2$. The interference term can be done in the same manner,

$$\begin{aligned}
W_{\mu\nu}^{\gamma Z} &= \sum_q \int d\xi q(\xi) \frac{E\delta(\xi-x)}{4\xi(k\cdot p)(p\cdot q)} \Big[(L_q+R_q)\frac{Q^\gamma_{\mu\nu}}{Q_q} + 2Q_q(L_q-R_q)\xi i\epsilon_{\alpha\mu\beta\nu}p^\alpha q^\beta \Big] \\
&= \underbrace{-\sum_q \frac{Q_q(L_q+R_q)}{2M} q(x)}_{-W_1^{\gamma Z}} \left(g_{\mu\nu} - \frac{q_\mu q_\nu}{q^2}\right) \\
&+ \underbrace{\sum_q \frac{Q_q x(L_q+R_q)}{M(p\cdot q)} q(x)}_{\frac{W_2^{\gamma Z}}{M^2}} \left(p_\mu - \frac{(p\cdot q)}{q^2}q_\mu\right)\left(p_\nu - \frac{(p\cdot q)}{q^2}q_\nu\right) \\
&+ \underbrace{\sum_q \frac{Q_q(L_q-R_q)}{2M(p\cdot q)} q(x)}_{\frac{W_3^{\gamma Z}}{2M^2}} i\epsilon_{\alpha\mu\beta\nu}p^\alpha q^\beta
\end{aligned}$$

and the structure functions W_1, W_2 and W_3 can be read

$$\begin{aligned}
W_1^\gamma &= \sum_q \frac{Q_q^2}{2M} q(x) & W_2^\gamma &= x\sum_q \frac{Q_q^2}{\nu} q(x) \\
W_1^Z &= \sum_q \frac{(L_q^2+R_q^2)}{M} q(x) & W_2^Z &= x\sum_q \frac{2(L_q^2+R_q^2)}{\nu} q(x) \\
W_3^Z &= \sum_q \frac{2(L_q^2-R_q^2)}{\nu} q(x) & & \\
W_1^{\gamma Z} &= \sum_q \frac{Q_q(L_q+R_q)}{2M} q(x) & W_2^{\gamma Z} &= x\sum_q \frac{Q_q(L_q+R_q)}{\nu} q(x) \\
W_3^{\gamma Z} &= \sum_q \frac{Q_q(L_q-R_q)}{\nu} q(x). & &
\end{aligned}$$

2.6 Cross section

In order to form the cross section, it is necessary to calculate the contractions of equation (29). The differential cross section should then be written in a Lorentz-invariant form using Q^2, propagator virtuality, and Bjorken x, momentum fraction, as differentials.

The differential cross section (29) can be written as

$$\frac{d^2\sigma}{dE'd\Omega} = \frac{E'}{16\pi^2 E}\frac{e^4}{q^4}\Big[L_\gamma^{\mu\nu}W_{\mu\nu}^\gamma + \frac{\eta^2}{4}L_Z^{\mu\nu}W_{\mu\nu}^Z - \eta L_{\gamma Z}^{\mu\nu}W_{\mu\nu}^{\gamma Z}\Big], \tag{45}$$

where the factor

$$\eta = \frac{g_Z^2}{e^2}\frac{2q^2}{q^2 - M_Z^2} \tag{46}$$

depicts the ratio of each contraction in terms of its couplings and propagators.

The contractions with leptonic tensors $L^{\mu\nu}W_{\mu\nu}$ are calculated in appendix B. The result for the fully symmetric γ term is

$$\begin{aligned} L_\gamma^{\mu\nu}W_{\mu\nu}^\gamma &= 2\Big[k'^\mu k^\nu + k'^\nu k^\mu - (k\cdot k')g^{\mu\nu}\Big] \qquad (47)\\ &\quad\times\Big[-W_1^\gamma(g_{\mu\nu} - \frac{q_\mu q_\nu}{q^2}) + \frac{W_2^\gamma}{M^2}(p_\mu - \frac{(q\cdot p)}{q^2}q_\mu)(p_\nu - \frac{(q\cdot p)}{q^2}q_\nu)\Big]\\ &= 4\Big[W_1^\gamma(k\cdot k') + \frac{W_2^\gamma}{M^2}\Big((k\cdot p)(k'\cdot p) - \frac{(k\cdot k')p^2}{2}\Big)\Big]. \qquad (48)\end{aligned}$$

The contractions involving Z boson have antisymmetric parts as well. The resulting forms are

$$\begin{aligned} L_Z^{\mu\nu}W_{\mu\nu}^Z &= 8(L_e^2 + R_e^2)\Big[W_1^Z(k\cdot k') + \frac{W_2^Z}{M^2}((k\cdot p)(k'\cdot p) - \frac{(k\cdot k')p^2}{2})\Big]\\ &\quad - 8(L_e^2 - R_e^2)\frac{W_3^Z}{2M^2}\frac{q^2}{2}\Big[(k\cdot p) + (k'\cdot p)\Big] \qquad (49)\\ L_{\gamma Z}^{\mu\nu}W_{\mu\nu}^{\gamma Z} &= 4(L_e + R_e)\Big[W_1^{\gamma Z}(k\cdot k') + \frac{W_2^{\gamma Z}}{M^2}((k\cdot p)(k'\cdot p) - \frac{(k\cdot k')p^2}{2})\Big]\\ &\quad - 4(L_e - R_e)\frac{W_3^{\gamma Z}}{2M^2}\frac{q^2}{2}\Big[(k\cdot p) + (k'\cdot p)\Big]. \qquad (50)\end{aligned}$$

Inserting the contractions to the cross section (45) and reordering the terms gives

$$\begin{aligned}\frac{d^2\sigma}{dE'd\Omega} =& \frac{E'}{16\pi^2 E}\frac{e^4}{q^4} \\ & 4\Big(\Big[\underbrace{W_1^\gamma + \eta^2\frac{(L_e^2+R_e^2)}{2}W_1^Z - \eta(L_e+R_e)W_1^{\gamma Z}}_{W_1}\Big](k\cdot k') \\ & +\Big[\underbrace{\frac{W_2^\gamma}{M^2} + \eta^2\frac{(L_e^2+R_e^2)}{2}\frac{W_2^Z}{M^2} - \eta(L_e+R_e)\frac{W_2^{\gamma Z}}{M^2}}_{\frac{W_2}{M^2}}\Big][(k\cdot p)(k'\cdot p) - \frac{(k\cdot k')p^2}{2}] \\ & -\Big[\underbrace{\eta^2\frac{(L_e^2-R_e^2)}{2}\frac{W_3^Z}{2M^2} - \eta(L_e-R_e)\frac{W_3^{\gamma Z}}{2M^2}}_{\frac{W_3}{2M^2}}\Big]\frac{q^2}{2}[(k\cdot p)+(k'\cdot p)]\Big). \end{aligned} \tag{51}$$

Structure factors W_1 and W_2 now consist of 3 terms, and W_3 only of 2 terms, the Z and γZ contributions. The DIS cross section in target rest frame now reads

$$\begin{aligned}&\frac{d^2\sigma}{dE'd\Omega} = \frac{E'}{4\pi^2 E}\frac{e^4}{q^4} \\ &\Big\{W_1(k\cdot k') + \frac{W_2}{M^2}\Big[(k\cdot p)(k'\cdot p) - \frac{(k\cdot k')p^2}{2}\Big] + \frac{W_3}{2M^2}\frac{q^2}{2}\Big[(k\cdot p)+(k'\cdot p)\Big]\Big\}. \end{aligned} \tag{52}$$

2.6.1 Coordinate transformations

The differentials dE' and $d\Omega$ in cross section can be converted into DIS differentials dQ^2 and dx using the following equalities:

$$\begin{aligned} Q^2 = -q^2 = 4EE'\sin^2\frac{\theta}{2} \qquad & d\Omega = 2\pi\sin\theta d\theta, \\ x = \frac{Q^2}{2(p\cdot q)} = \frac{2EE'\sin^2\frac{\theta}{2}}{M(E-E')} \qquad & y = \frac{p\cdot q}{p\cdot k} = \frac{E-E'}{E}. \end{aligned}$$

The coordinate transformation from base (E',Ω) to (x,y) is done by multiplying by Jacobian determinant in the following way:

$$\frac{d^2\sigma}{dE'd\Omega} = \det[J(E',\Omega)]\frac{d^2\sigma}{dxdy} \Leftrightarrow \frac{d^2\sigma}{dxdy} = \det[J(E',\Omega)]^{-1}\frac{d^2\sigma}{dE'd\Omega}$$

$$J(E',\Omega) = \begin{bmatrix} \frac{\partial x}{\partial E'} & \frac{\partial x}{\partial \Omega} \\ \frac{\partial y}{\partial E'} & \frac{\partial y}{\partial \Omega} \end{bmatrix},$$

where the partial derivatives are

$$\frac{\partial x}{\partial E'} = \frac{2E\sin^2\frac{\theta}{2}}{M}\frac{E}{(E-E')^2}$$

$$\frac{\partial x}{\partial \Omega} = \frac{\partial x}{2\pi\sin\theta\partial\theta} = \frac{EE'}{M(E-E')\pi\sin\theta}\underbrace{\sin\frac{\theta}{2}\cos\frac{\theta}{2}}_{\frac{1}{2}\sin\theta} = \frac{EE'}{2\pi M(E-E')}$$

$$\frac{\partial y}{\partial E'} = -\frac{1}{E} \qquad \frac{\partial y}{\partial \Omega} = 0$$

and the Jacobian determinant for this transformation is

$$\det[J(E',\Omega)]^{-1} = \left(\frac{E'}{2\pi M(E-E')}\right)^{-1} = \frac{2\pi M(E-E')}{E'}.$$

Doing this again for a transormation $(x,y) \Rightarrow (x,Q^2)$

$$\det[J(x,Q^2)] = \begin{vmatrix} \frac{\partial x}{\partial x} & \frac{\partial x}{\partial Q^2} \\ \cancel{\frac{\partial y}{\partial x}}^{\,0} & \frac{\partial y}{\partial Q^2} \end{vmatrix} = \frac{\partial y}{\partial Q^2} = \frac{1}{2x(p\cdot k)} \tag{53}$$

gives the full transformation as

$$\frac{d^2\sigma}{dxdQ^2} = \frac{1}{2x(p\cdot k)}\frac{d^2\sigma}{dxdy} = \frac{2\pi M(E-E')}{2x(p\cdot k)E'}\frac{d^2\sigma}{dE'd\Omega}. \tag{54}$$

The cross section in Lorentz-invariant DIS quantities is then

$$\frac{d^2\sigma}{dxdQ^2} = \frac{(E-E')}{4\pi E^2 x}\frac{e^4}{q^4}$$
$$\left\{W_1(k\cdot k') + \frac{W_2}{M^2}\left[(k\cdot p)(k'\cdot p) - \frac{(k\cdot k')p^2}{2}\right] + \frac{W_3}{2M^2}\frac{q^2}{2}\left[(k\cdot p) + (k'\cdot p)\right]\right\}. \tag{55}$$

2.6.2 Neutral-current DIS cross section and structure functions

Defining dimensionless structure functions F_i and using some manipulations

$$\begin{aligned} F_1(x,Q^2) &= MW_1 & F_2(x,Q^2) &= \nu W_2 \\ -q^2 = -2(k\cdot k') &= 4EE'\sin^2\tfrac{\theta}{2} = -2EE'(1-\cos^2\tfrac{\theta}{2}) & &= Q^2 = 2MEyx \\ x &= \tfrac{Q^2}{2MEy} & y &= \tfrac{\nu}{E} \\ (p\cdot k') &= ME' & \alpha &= \tfrac{e^2}{4\pi} \end{aligned} \tag{56}$$

gives the first two terms of cross section as

$$\begin{aligned} &\frac{(E-E')}{4\pi xE^2}\frac{e^4}{Q^4}\Big[\frac{Q^2}{2}W_1 + \frac{W_2}{M^2}(M^2EE' - M^2EE'\sin^2\frac{\theta}{2})\Big] \\ =&\frac{\nu e^4}{4\pi xQ^4}\frac{E'}{E}\Big[\frac{Q^2}{2MEE'}F_1 + \Big(1-\frac{Q^2}{4EE'}\Big)\frac{F_2}{\nu}\Big] \\ =&\frac{e^4}{4\pi xQ^4}\Big[\frac{Q^2\nu}{2ME^2}\frac{\nu}{yE}F_1 + \Big(\frac{E'}{E}-\frac{Q^2}{E^2}\Big)F_2\Big] \\ =&\frac{16\pi^2\alpha^2}{4\pi xQ^4}\Big[\underbrace{\frac{Q^2}{2yME}}_{x}\underbrace{\frac{\nu^2}{E^2}}_{y^2}F_1 + \Big(\frac{E'}{E}\underbrace{\uparrow}_{1-\frac{E}{E}} - \frac{2M\nu x}{4E^2}\Big)F_2\Big] \\ =&\frac{4\pi\alpha^2}{xQ^4}\Big[xy^2F_1 + \Big(1-\underbrace{\frac{E-E'}{E}}_{y} - \frac{M^2yx}{2ME}\Big)F_2\Big] \\ =&\frac{1}{2MEx}\frac{4\pi\alpha^2}{xyQ^2}\Big[xy^2F_1 + \Big(1-y-\frac{M^2x^2y^2}{Q^2}\Big)F_2\Big]. \end{aligned}$$

The W_3 term is modified similarly by defining $F_3(x,Q^2) = \nu W_3$

$$\begin{aligned} &\frac{(E-E')e^4}{4\pi xQ^4}\frac{E'}{E}\Big(\frac{W_3}{2M^2}\frac{q^2}{2}[(k\cdot p)+(k'\cdot p)]\Big) = \frac{4\pi\alpha^2\nu}{Q^4xE^2}\Big(\frac{W_3}{4M}Q^2(E+E')\Big) \\ =&\frac{4\pi\alpha^2}{xQ^4}\frac{Q^2}{4ME^2}(E+E')F_3 = -\frac{4\pi\alpha^2}{xQ^4}\frac{EQ^2}{4ME^2}(1+\frac{E'}{E})F_3 \\ =&-\frac{4\pi\alpha^2}{xQ^4}\frac{2ME^2yx}{4ME^2}(2-y)F_3 = -\frac{4\pi\alpha^2}{xQ^4}(1-\frac{y}{2})yxF_3 \\ =&-\frac{1}{2MEx}\frac{4\pi\alpha^2}{xyQ^2}(y-\frac{y^2}{2})xF_3. \end{aligned}$$

The minus sign of W_3 term cancels, and $2ME = s - M^2$ is Lorentz-invariant as well. Putting the terms together gives the final neutral-current DIS cross section

$$\frac{d^2\sigma}{dxdQ^2} = \frac{1}{x(s-M^2)}\frac{4\pi\alpha^2}{xyQ^2}\Big[y^2xF_1 + \Big(1 - y - \frac{M^2x^2y^2}{Q^2}\Big)F_2 + \Big(y - \frac{y^2}{2}\Big)xF_3\Big]. \quad (57)$$

The neutral-current structure functions can be read from equation (51). The equations correspond to those of Particle Data Group [7] by making the substitutions

$$\eta' = 2\eta, \quad \eta'^2 = 4\eta, \quad W_i^{Z\prime} = \frac{1}{4}W_i^Z, \quad F_i^{Z\prime} = \frac{1}{4}F_i^Z. \quad (58)$$

The equality still holds, and the neutral-current structure functions are (omitting the apostrophe)

$$\begin{aligned} F_2^{\mathrm{NC}} = 2xF_1^{\mathrm{NC}} &= F_2^\gamma + \eta^2\frac{(L_e^2 + R_e^2)}{2}F_2^Z - \eta\frac{(L_e + R_e)}{2}F_2^{\gamma Z} \\ F_3^{\mathrm{NC}} &= \eta^2\frac{(L_e^2 - R_e^2)}{2}F_3^Z - \eta\frac{(L_e - R_e)}{2}F_3^{\gamma Z}, \end{aligned} \quad (59)$$

where

$$\begin{aligned} F_2^\gamma(x,Q^2) &= x\sum_q Q_q^2(q+\overline{q}) & \eta &= \frac{g_Z^2}{e^2}\frac{4q^2}{q^2 - M_Z^2} \\ F_2^Z(x,Q^2) &= x\sum_q \frac{(L_q^2 + R_q^2)}{2}(q+\overline{q}) & F_3^Z(x,Q^2) &= \sum_q \frac{(L_q^2 - R_q^2)}{2}(q-\overline{q}) \\ F_2^{\gamma Z}(x,Q^2) &= x\sum_q Q_q(L_q + R_q)(q+\overline{q}) & F_3^{\gamma Z}(x,Q^2) &= \sum_q Q_q(L_q - R_q)(q-\overline{q}), \end{aligned} \quad (60)$$

and the sum goes over all quark flavors, $q = d, u, s, c, b, t$. Since this is the final form for these equations, the contributions for antiquarks are added as well. In the calculation for antiquarks, the only difference is in the invariant amplitude $\mathcal{M}$. The Feynman rules for external antifermions are given in appendix A, and results in swapping the parton momentums $\hat{p}$ and $\hat{p}'$ in $\mathcal{M}$. As the structure functions F_1 and F_2 contain only symmetrical parts, this change has no effect on them. Ultimately, the only differences are that the structure function F_3 has a minus sign, so the PDFs for antiquarks are denoted by $\overline{q}$.

2.7 Monte Carlo methods

The essential tool to build the simulation is Monte Carlo sampling from a distribution. It uses known probability distribution functions and random numbers to draw samples according to the probability dictated by the studied distribution. The distribution in this case is the cross section (57), and the samples drawn are pairs of x and Q^2. The basic idea is to make a random guess from the domain which defines the phase space Ω, and accept or reject it. The condition to accept the sample is proportional to the distribution itself. The importance sampling method is used to make better initial guesses. This technique picks the guesses from a limiting function $g(x, Q^2)$ which covers the cross section from above, $g(x, Q^2) \geq \frac{d^2\sigma}{dxdQ^2} \; \forall \; (x, Q^2) \in \Omega$. In case the limiting function can be separated as $g(x, Q^2) = g_1(x)g_2(Q^2)$, the values can be picked analytically from the functions g_i if they are integrable and the primitive function G_i is invertible in the domain of interest. The analytical method is given by the equation

$$\int_{x_{\min}}^{x} g(x')dx' = R \int_{x_{\min}}^{x_{\max}} g(x')dx', \tag{61}$$

where $R \in]0, 1[$ is a random number generated from a flat distribution. The connection of x and R is clear if we consider the left-hand side to be the integral from $x_{\min}$ to some random value x. The right-hand side is then the fraction R of the whole integral. Solving this for x gives

$$x = G^{-1}\Big[G(x_{\min}) + R\Big(G(x_{\max}) - G(x_{\min})\Big)\Big]. \tag{62}$$

Once both of the values are picked, the cross section is calculated. Then a new random number R is generated, and the values are accepted if

$$\frac{d^2\sigma}{dxdQ^2} > Rg(x, Q^2). \tag{63}$$

With a suitable limiting function $g(x, Q^2)$, this sampling algorithm produces pairs of x and Q^2 from the differential cross section.

3 Simulation

Lepton-quark -scattering sub-process in the parton level is elastic 2-to-2 scattering, so it only needs two independent variables to fix the kinematics, x and Q^2 in this case. With the initial-state particle 4-vectors chosen to move along the z direction, the process can be simulated by constructing the final-state 4-vectors using the sampled quantities, from which any other quantity can be derived. The scattering angle is chosen to be between the z and x axes, and the transverse momentum is set to point to x direction. This doesn't change the physics, only the coordinates, since the azimuthal angle is independent of the cross section. The implementation handles the phase space, quark flavor sampling and kinematics as well. It also takes the quark masses into account.

The necessary initial parameters are electron and proton beam energies E and E_p and minimum propagator virtuality Q^2_{min}. Some optional parameters are maximum number of sampled events N_{target} and maximum propagator virtuality Q^2_{max}. These set initial conditions and the kinematic region.

3.1 Limiting function

The sampling starts by drawing values of x and Q^2 from the limiting function $g(x,Q^2)$. To achieve a sufficient efficiency, the function should imitate the behaviour of $d\sigma$. A suitable limiting function for the studied cross section is found to be

$$g(x,Q^2) = Ag_1(x)g_2(Q^2) = Ax^{-a}(Q^2)^{-b}, \tag{64}$$

where the constant $A = d\sigma_{\text{max}}x^a(Q^2)^b$ sets the maximum value of the limiting function equal to the maximum value of cross section. The exponents a and b are picked with the use of a optimization algorithm.

The efficiency of the MC method can be evaluated from

$$\frac{\int_\Omega \frac{d^2\sigma}{dxdQ^2}}{\int_\Omega g(x,Q^2)}, \tag{65}$$

which is the ratio of the 3-dimensional volumes in a $(x, Q^2, \frac{d^2\sigma}{dxdQ^2})$ coordinate system. To make use of this, the cross section was calculated in a logarithmic grid of x and Q^2 in the region Ω. Since "most" of the cross section resides in small x and Q^2 values, a logarithmic spacing was used. The sum of the ratio of these values represents the inverse of the efficiency:

$$\sum_{(x,Q^2)\in\Omega} \frac{\frac{d^2\sigma}{dxdQ^2}(\Omega)}{g(\Omega)}. \tag{66}$$

To maximize sampling efficiency, this sum can be minimized in terms of the exponents a and b of the limiting function. However, the graphs of the functions should not cross, so the ratio is set to infinity if $g(x, Q^2) - \frac{d^2\sigma}{dxdQ^2} < 0$. This way the minimum of the sum function is found only when the functions do not cross.

A minimizing algorithm was used with the initial guesses $a = 1.1$ and $b = 1.5$. The algorithm used is the Nelder-Mead simplex algorithm, implemented in the Python library SciPy as `scipy.optimize.fmin()`. These initial values were selected by hand, by studying the behaviour of the cross section. The resulting exponents were $a \approx 1.1$ and $b \approx 2.1$. To ensure that the limiting function stays above the cross section, an extra factor of 1.01 was added to $g(x,Q^2)$. The minimizing algorithm doesn't use information about the derivatives, so the result highly depends on the initial guess. The MC method prohibits the use of $a = 1$, since the exponent would have a division by zero, so the initial guesses cannot be exactly one. Also, since the exponents are negative, the starting points of x and Q^2 cannot be exactly zero.

3.2 Monte Carlo sampling

Using the analytic method (62) separately for the functions g_1 and g_2 gives

$$x = \left[x_{\min}^{1-a} + R_x(1 - x_{\min}^{1-a})\right]^{\frac{1}{1-a}}$$
$$Q^2 = \left[(Q^2_{\min})^{1-b} + R_{Q^2}(1 - (Q^2_{\min})^{1-b})\right]^{\frac{1}{1-b}}.$$

The kinematic limits are set by $Q^2_{\min} = 1$ GeV^2 and $x_{\min} = Q^2_{\min}/(s - M^2 - m_e^2)$, and the maximum value $Q^2_{\max} = s - M^2 - m_e^2$ is dictated by the initial beam energies. The propagator virtuality Q^2 and the Bjorken x are drawn this way. The values are

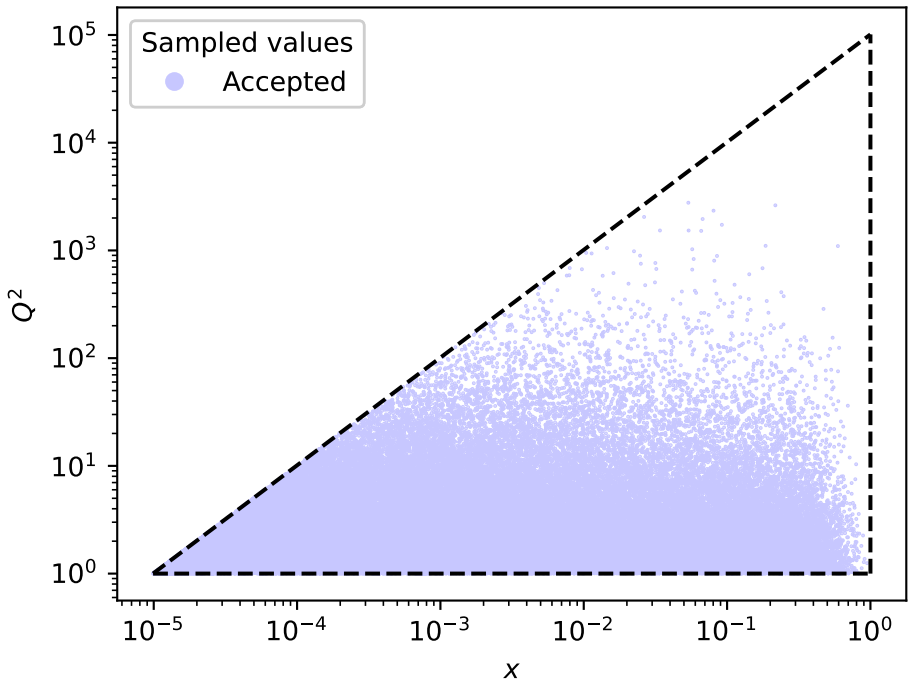

Figure 4. $N = 100000$ sampled values in the (x,Q^2) domain with logarithmic axes. The domain is set by $Q^2_{\text{min}} = 1$ GeV^2 and $x_{\text{min}} = Q^2/(s - M^2 - m_e^2)$.

rejected if they are outside the kinematically allowed region,

$$x \leq Q^2/(s - M^2 - m_e^2), \tag{67}$$

or if the accept-condition (63) is not met. The limit for the phase space is derived from the definition of inelasticity $y \in [0,1]$ as follows:

$$y = \frac{q \cdot p}{k \cdot p}, \qquad x = \frac{Q^2}{2(q \cdot p)} = \frac{Q^2}{2y(k \cdot p)} \overset{y=1}{\Rightarrow} \quad x_{\text{min}} = \frac{Q^2}{s - M^2 - m_e^2}. \tag{68}$$

In order to obtain a separable function $g(x,Q^2) = g_1(x)g_2(Q^2)$, the limits x_{min} and Q^2_{max} cannot depend on each other. Figure 4 presents the sampled points in the phase space Ω. From the figure one can deduce that most of the events happen at low x and Q^2 values. These accepted points are then used to build the kinematics and construct the particle four-vectors. The domain begins at the user-defined Q^2_{min}, and the hypotenuse of this triangle is given by equation (67).

Computation of the differential cross section is done with the use of PDFs from PYTHIA libraries, namely the LHAGrid1 approach [5] which interpolates the

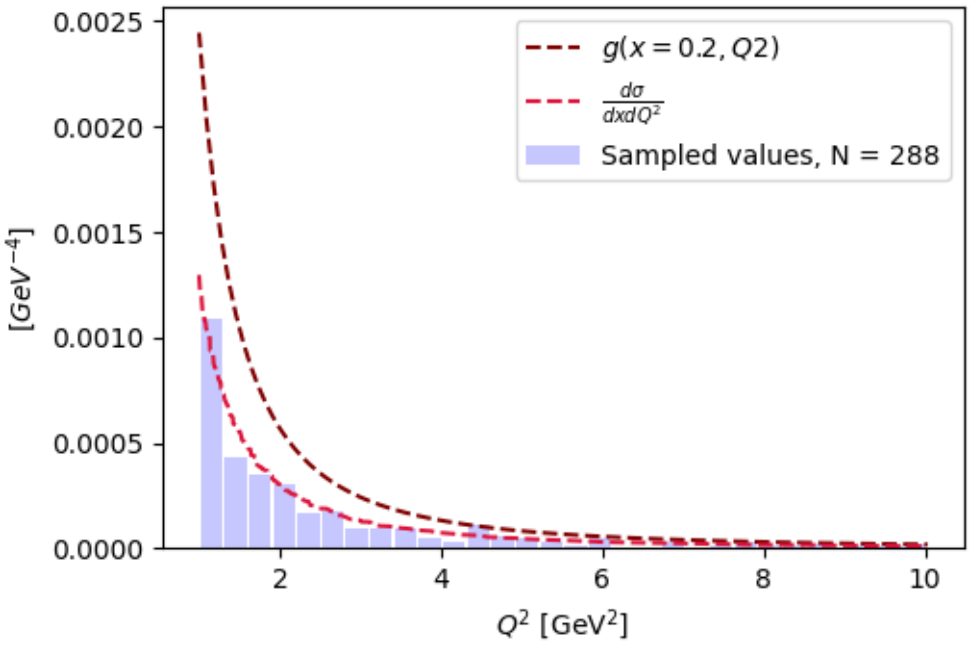

Figure 5. The sampled values from an x interval of 0.2 ± 0.01 as a histogram. The cross section is drawn in the sampled points and the limiting function in the Q^2 interval. The histogram is normalized so that its integral is equal to that of $d\sigma$.

LHAPDF6 [8] set. The PDF used is the default option NNPDF2.3 [9]. The function `double PDF::xf(int id, double x, double Q2)` of the PDF object returns x times the PDF $q(x, Q^2)$ of the structure functions (60). The quark indices `id` in PYTHIA are $1, 2, 3, 4, 5, 6$ for quarks in the order d, u, s, c, b, t, and negative for corresponding antiquark. The differential cross section (57) is computed with these PDFs and physical constants which are presented in appendix A. By drawing a new random number and comparing the values of R times the limiting function and the cross section, the probability to accept the values is proportional to the cross section itself. Figure 5 depicts a "slice" of the cross section in a small interval of $x = 0.2 \pm 0.01$. The differential cross section and the limiting function are plotted as well to illustrate the Monte Carlo method. The tries are done as a point below $g(x, Q^2)$, and if this point is under the graph of $d\sigma$, it is accepted and added to the histogram. The limiting function is larger than the cross section, and the sampling algorithm reproduces the desired distribution.

Quark flavor sampling is the next step in the program. It can be done by calculating the cross section as a sum of each quark flavor contribution, drawing

once again a new random number R_q and comparing this to the ratio

$$\sum_q \frac{d\sigma_q}{d\sigma} > R_q. \tag{69}$$

The sum goes over all quarks and antiquarks in the order $q = d, u, s, c, b, t, \bar{d}, \bar{u}, \bar{u}, \bar{s}, \bar{c}, \bar{b}, \bar{t}$. The term which sets this ratio greater than R_q defines the quark type.

3.3 Kinematics

Although the parton has a momentum of $\hat{p} = xp$ in the parton model, this is only valid in the infinite momentum frame where masses are negligible. In order to get the correct quark masses into the simulation, the vector $\hat{p}$ has to be solved some other way. Here we use the p^+ momentum that allows to set the quark into its mass shell and the definition of Lorentz-invariant x,

$$x = \frac{\hat{p}_+}{p_+} = \frac{|\hat{p}_z| + \hat{E}}{|p_z| + E} \tag{70}$$

$$\Leftrightarrow \hat{E} = \frac{x}{2}\Big((|p_z| + E_p) + \frac{\hat{m}^2}{x^2(|p_z| + E_p)}\Big). \tag{71}$$

The momentum is then given as usual, by the dispersion relation (9).

With the particles and quantities set, the kinematics are then built with the initial state four-vectors

$$k = [0, 0, k_z, E] \quad \text{and} \quad \hat{p} = [0, 0, \hat{p}_z, \hat{E}]. \tag{72}$$

The collision kinematics are easily calculated in the lepton-parton center of momentum system (CMS). This is achieved by Lorentz-boosting the vectors

$$k_z^{\mathrm{CMS}} = -\hat{p}_z^{\mathrm{CMS}} = \gamma(k_z - vE) = -\gamma(\hat{p}_z - v\hat{E})$$
$$\Leftrightarrow v = \frac{k_z + \hat{p}_z}{E + \hat{E}}, \text{ where } \quad \gamma = \frac{1}{\sqrt{1 - v^2}}.$$

Assuming that transverse momentum is along the x-axis, the final state four-vectors

are obtained as

$$\begin{aligned} k' &= [p^{\mathrm{CMS}} \sin\theta^{\mathrm{CMS}}, \quad 0, \quad p^{\mathrm{CMS}} \cos\theta^{\mathrm{CMS}}, \quad E'^{\mathrm{CMS}}] \\ \hat{p}' &= [-p^{\mathrm{CMS}} \sin\theta^{\mathrm{CMS}}, \quad 0, \quad -p^{\mathrm{CMS}} \cos\theta^{\mathrm{CMS}}, \quad \hat{E}'^{\mathrm{CMS}}], \end{aligned} \tag{73}$$

where the CMS quantities are

$$\begin{array}{ll} E'^{\mathrm{CMS}} = \frac{\hat{s}+m_e^2-\hat{m}^2}{2\sqrt{\hat{s}}} & \hat{E}'^{\mathrm{CMS}} = \frac{\hat{s}-m_e^2+\hat{m}^2}{2\sqrt{\hat{s}}} \\ p^{\mathrm{CMS}} = \frac{\sqrt{\lambda(s,m_e^2,\hat{m}^2)}}{2\sqrt{\hat{s}}} & \cos\theta^{\mathrm{CMS}} = 1 + \frac{2\hat{s}\hat{t}}{\lambda(s,m_e^2,\hat{m}^2)} \\ \hat{s} = (k+\hat{p})^2 \quad \hat{t} = t = -Q^2 & \lambda(x,y,z) = x^2+y^2+z^2-2xy-2xz-2yz \end{array} . \tag{74}$$

Then the vectors are boosted back to the lab frame. The scattering event simulation is completed, and any quantity that can be constructed from the four-momenta can be considered, such as the quantities (8) and the transverse momentum $p_{\mathrm{T}} = \sqrt{p_x^2 + p_y^2}$.

In the scattering, the proton is broken down and creates new particles. The mass and energy of the proton and the struck quark are transformed to masses and energies of new particles, which might not be detected in experiments. The invariant mass of these particles is W. This has a maximum value at $q_{\max} = (k-k')_{\max} = k$, which describes an event where the electron gives all of its momentum to the propagator. Omitting the masses, the value can be computed as

$$\begin{aligned} W^2 =& (p+q)^2 = (E_p+E_q)^2 - (\vec{p}+\vec{q})^2 \\ =& E_P^2 + E_q^2 + 2E_P E_q - (|\vec{P}|^2 + |\vec{q}|^2 + 2\vec{P}\cdot\vec{q}) \\ \underbrace{W^2_{\max} \approx}_{|\vec{p}|\approx E_p, |\vec{q}|\approx E_q = E} & 2E_pE - 2E_pE\cos\theta = 4E_pE \\ \Rightarrow W_{\max} =& \sqrt{4E_pE} = 318.119 \text{ GeV}. \end{aligned} \tag{75}$$

The coordinates are chosen in a way that the transverse momentum p_{T} of the particles is along the x-axis. Getting the x and Q^2 back from the final state vectors gives some insight on the functionality of the simulation and kinematics. The program has some measures to handle faulty events. Firstly, the four-momentum has to be conserved. This might fail in cases where numerical precision is lost. Secondly, the difference in sampled and reconstructed x must not exceed a given threshold, 0.001 as default. The event is marked as failed if either of these faults are present.

The program was ran with beam energies set to match DIS data measured in

DESY-HERA collider [1]. The parameters were

$$\begin{array}{lll} E = 27.5 \text{ GeV} & E_p = 920 \text{ GeV} & Q^2_{\text{min}} = 1 \text{ GeV}^2 \\ a = 1.1 & b = 2.1 & \end{array} .$$

The propagator virtuality limit sets the low end of phase space, and the exponents were selected to efficiently sample in this region, with the use of optimizing algorithm presented in section 3.1.

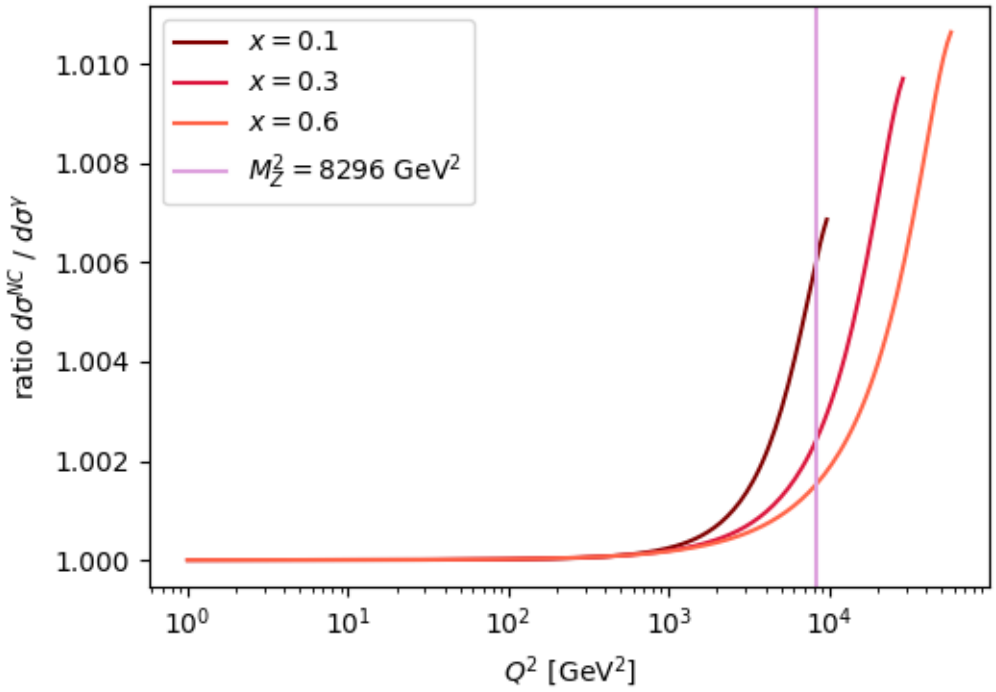

Figure 6. The ratio of NC interaction cross section by photon interaction cross section with different fixed x. Mass of the Z boson squared is pictured as a straight line.

4 Results

With the cross section implemented numerically, values of NC interaction and purely photonic interaction were gathered. Figure 6 illustrates the effect of adding Z boson interaction to the photon exchange process. The cross section is essentially the same until $Q^2 \sim M_Z^2$. Then the interactions are energetic enough to produce a Z boson, and the cross section is less than 1% larger. The lines end at the maximum Q^2 values, determined by the fixed x. This result is important for the sampling method. As the effects of Z boson interaction are minimal, there is no need to handle the large Q^2 region differently. The same limiting function is suitable for both NC interaction as well as purely photonic interaction.

Simulations and the PYTHIA program were executed to gather $N = 100000$ sampled events, with results presented in figures 8 through 12. The quantities are explained in equation (8). The results were gathered from the presented simulation software with quark masses set equal to ones used by PYTHIA, with the command `pythia.particleData.m0("quark index")`. The masses that PYTHIA use for the quarks are $m_d = m_u = 0.33$ GeV, $m_s = 0.5$ GeV, $m_c = 1.5$ GeV and $m_b = 4.8$ GeV. The distributions are normalized to sampled total cross section. This means that the heights of the lines indicate the value of cross section, differential in the quantity in question. The total cross section is gathered by MC sampling, sort of as a by-product. Approximation for the integral of $\frac{d^2\sigma}{dxdQ^2}$ in equation (65) is given by

$$\begin{aligned} \sigma &= \int_{x_{\min}}^{1} \int_{1}^{Q^2_{\max}} \frac{d^2\sigma}{dxdQ^2}\, dx\, dQ^2 \;\approx\; V\, \frac{N_{\text{accepted}}}{N} \\ &= \int_{x_{\min}}^{1} \int_{1}^{Q^2_{\max}} g(x,Q^2)\, dx\, dQ^2\, \frac{N_{\text{accepted}}}{N}, \end{aligned} \tag{76}$$

where N_{accepted} is the number of accepted tries and N the total number of tries and V the volume of the sampled region, equal to the integral of $g(x, Q^2)$. Limits of the phase space are given in section 3.2. Error of the approximation decreases as $\sim 1/\sqrt{N}$ with increasing number of tries. Gathered histograms are then normalized by multiplying by total cross section and dividing by bin width and number of

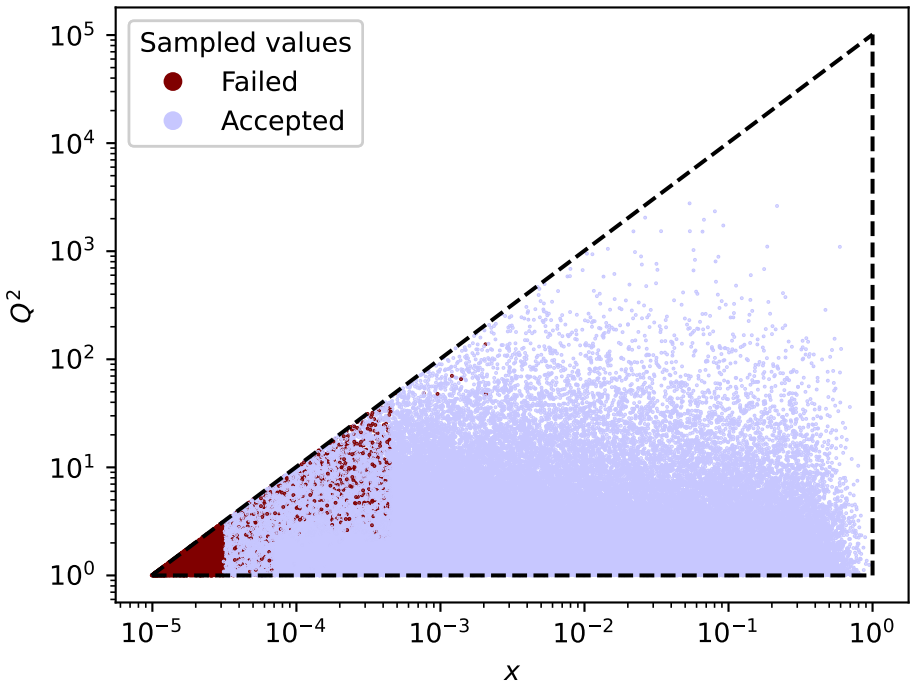

Figure 7. N = 100000 sampled values, with accepted and failed tries. The event is set to fail if the difference in sampled and reconstructed x is over 0.001.

tries. As the simulation works in natural units, the conversion factor of GeV^{-2} to millibarns (mb) is 2.568. Doing this for the presented simulation, and getting an equivalent value calculated by PYTHIA resulted in total cross sections of 0.00141 mb and 0.00133 mb respectively. There is a slight difference in these, and it's effect can be seen in the following figures.

Adding the quark masses introduced a problem in the kinematics of the simulation. The assumption $\hat{p} = xp$ doesn't hold in any other frame than the infinite momentum frame of frame of the proton as this does not set the quark into it's mass shell. To address this problem, the parton vector was solved from another definition of x. This however led to a problem in the calculated x when the sampled x was smaller than $\hat{m}/E_p$. These events are not energetic enough to produce a sampled quark on its mass-shell, and led to different values when the x was constructed from the four-vectors. This effect can be seen in figure 7, where the failed events produce cutoffs for different quarks. The lowest x values failed, with the cutoff proportional to up and down quark masses. The next cutoff is for the strange quark, and the last visible one for the charm quark. It is also apparent that the resolution power has to

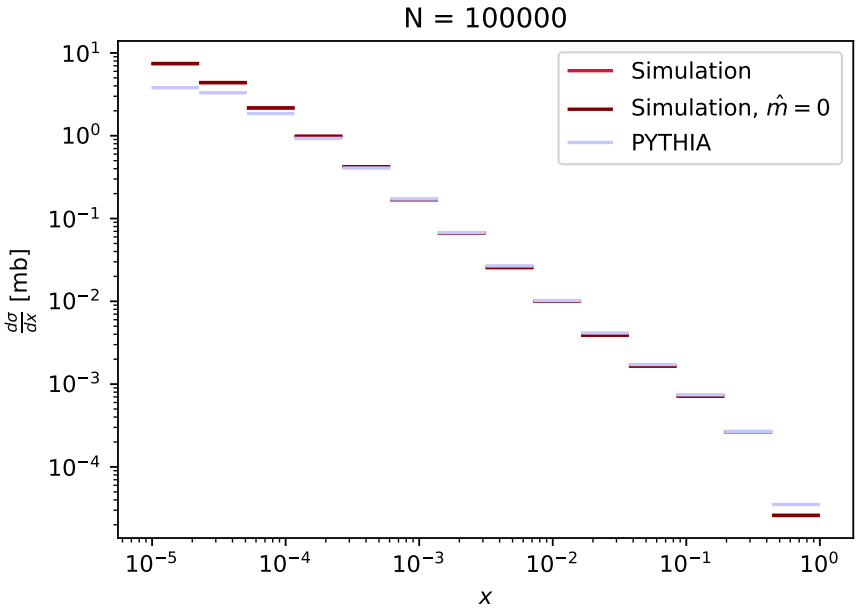

Figure 8. Sampled x values from the simulation with and without quark masses, and from PYTHIA. Logarithmic axes are used for both x and y direction. The distributions are normalized to the sampled total cross section.

be more than $Q^2 = 1$ GeV^2 in order to have heavier quarks in the interaction, as there is a horizontal cutoff in the phase space as well.

Sampled x values are presented in figure 8, with logarithmic axes to better visualize the distribution. The result indicates that most of the events happen at small x values, as was expected. Comparing the graphs of the simulation and PYTHIA event generator, they agree at larger values but differ at very small values of x. These events have proved to be the most problematic in a numerical implementation, and the PYTHIA DIS program has large differences in the sampled x and reconstructed x of the events at small x as well.

An important result can be seen in the Q^2 distribution, figure 9. The PYTHIA main program samples values lower than what was desired, with the parameter `Q2min` set to 1 GeV^2. The simulation, however, bypasses this problem entirely, and no events with Q^2 smaller than 1 GeV^2 were sampled. The cross section seems to be somewhat inversely proportional to the virtuality, which is evident in the expression (57) as well. The presented simulation uses a fixed seed for random number generator, so the sampled x and Q^2 are identical for executions with massive and massless quarks.

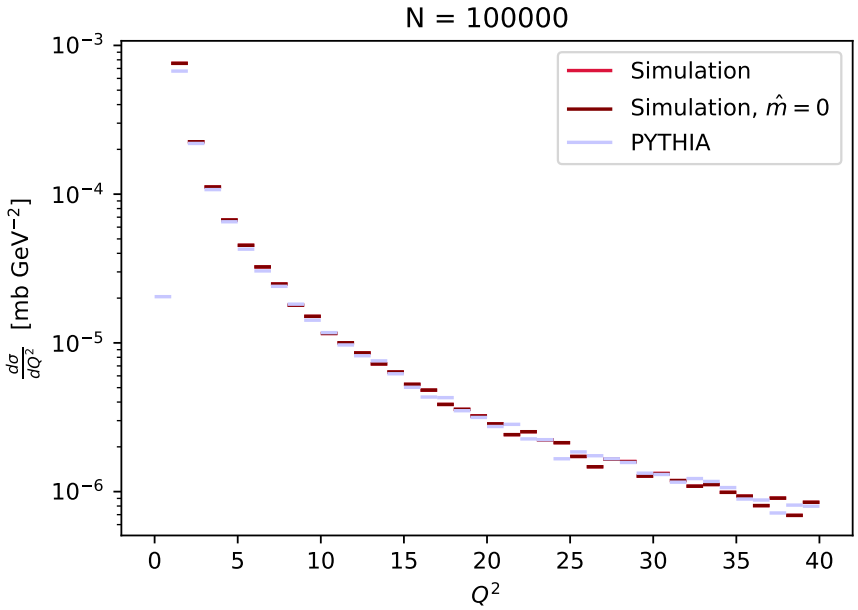

Figure 9. Sampled Q^2 values ranging from 0 to 40 GeV^2 from the presented simulation as well as PYTHIA event generator, normalized to sampled total cross section. A logarithmic y-axis is used.

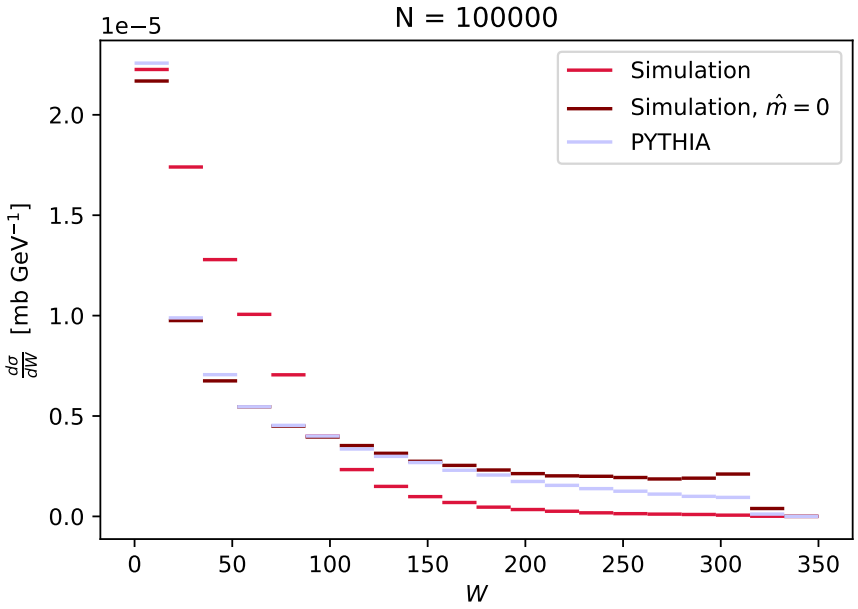

Figure 10. Values of invariant mass W of the remaining system of particles X, obtained from the constructed 4-vectors of the simulation and PYTHIA. Normalized to sampled total cross section.

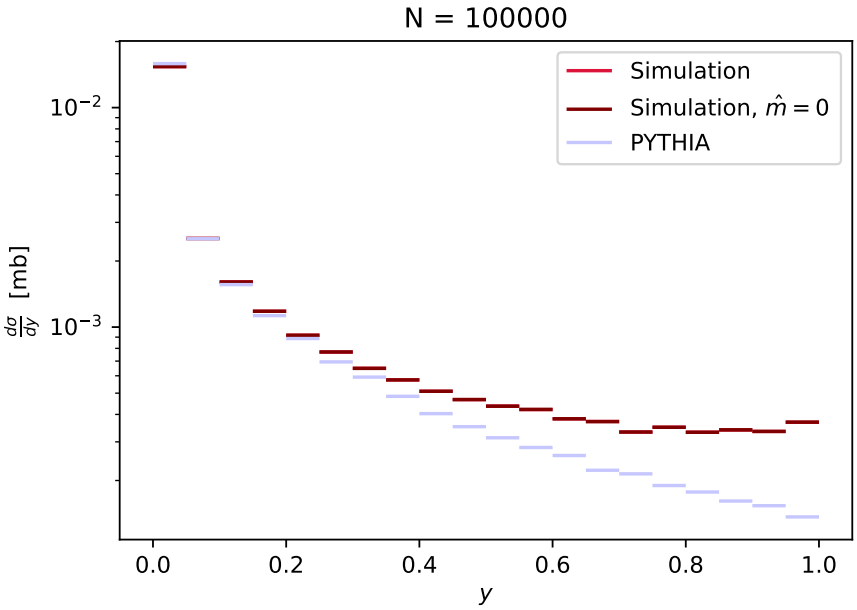

Figure 11. Inelasticity y calculated from the sampled values of the simulation, and from the constructed four vectors of PYTHIA. Normalized to sampled total cross section.

Since the invariant mass of the photon-proton system is proportional to the virtuality, it follows that the distribution 10 has an inversely proportional behaviour to the cross section. There is a cut off somewhere around 320 GeV, which is consistent with equation (75). The results without quark masses are similar, but there is a clear effect in this distribution when the quark masses are added to the simulation. There seems to be more events with small W and less events with high W.

The inelasticity distributions of figure 11 are plotted on a logarithmic y-axis. The simulation results are the same for massless and massive quarks, since these are calculated from the sampled values. There is a clear difference at large-y region with the values from PYTHIA.

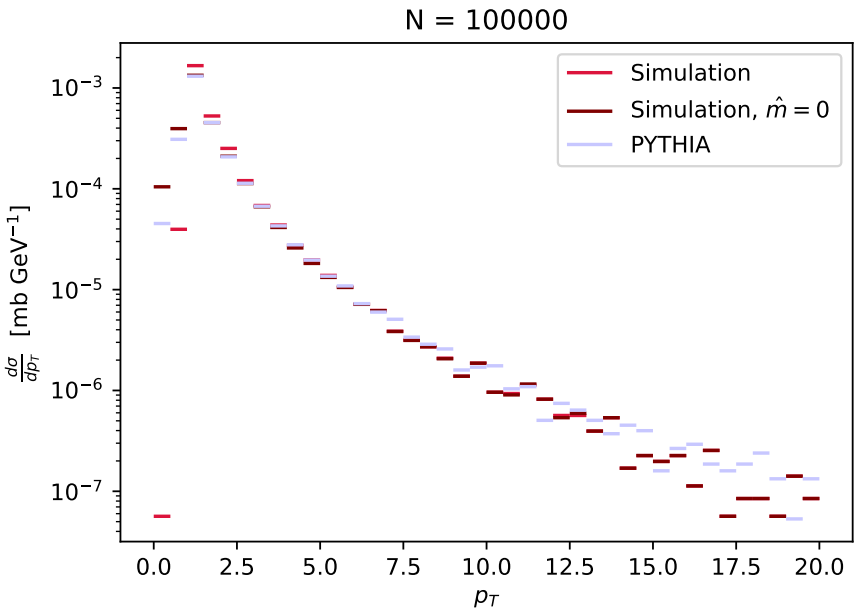

Figure 12. Transverse momentum $\hat{p}'_{\mathrm{T}}$ of the scattered parton ranging from 0 to 15 GeV, from the constructed four-vectors of the simulation and PYTHIA. Normalized to sampled total cross section.

As the quark is struck, it gains momentum perpendicular to the beam axis z. This transverse momentum has the same magnitude but opposite direction for the electron. The p_{T} distribution of the electron is therefore identical to that of the struck quark, figure 12. This distribution is also plotted in a logarithmic y-axis for clarity. There is a clear peak at $\hat{p}'_{\mathrm{T}} \sim 2$ GeV, and the distribution indicates that the scattering favors events with small transverse momentum. The peak is dependent on the limits of Q^2. A difference can be seen in the lowest values of $\hat{p}'_{\mathrm{T}}$ for the massive and massless case. Adding the quark masses results in noticeably less events with $\hat{p}'_{\mathrm{T}}$ smaller than 2 GeV, but slightly more events with $\hat{p}'_{\mathrm{T}}$ around 2.5 GeV.

5 Conclusions

Monte Carlo event generators are beneficial for the research of high-energy physics, as they can help in the planning of collider experiments, and predict what kind of results are expected. The vision of making an event generator for PYTHIA, solely focusing on lepton-nucleon DIS, led to the approach of Monte Carlo sampling of Bjorken x and virtuality Q^2 from the cross section of the process. The simulation built handles only the parton level sub-process, where the lepton scatters off a quark.

The NC DIS cross section can be derived with the use of Feynman rules. The parton model depicts the scattering process as interactions between the lepton and a quark, and enables the identification of structure functions in terms of parton distribution functions. The contribution of Z boson in the process is minimal compared to the photon contribution, so the scattering events are highly dominated by photon interaction. Using the derived expression as the distribution for Monte Carlo sampling enables the selection of x and Q^2 with a similar probability to emerge as in scattering experiments. The importance sampling method proves to be a successful option with a suitable limiting function, which was improved with an optimizing algorithm, so it could handle different kinematic regions. It makes no difference whether the Z contribution is included for this kind of MC sampling or not. Taking care of the kinematic limits and quark sampling, the parton level process is simulated successfully, and various variables of interest are obtained. With the option to optimize the limiting function, the MC efficiency is great for a wide range in the phase space, but the parameters need to be separately fitted.

Building the sampling and kinematics in the presented way conserves the x and Q^2 completely for massless quarks. This is a desirable result, as the PYTHIA program has the unwanted effect of getting different values for the quantities. However, adding the masses to the quark four-vectors proved to be problematic. The propagator $q = k - k'$ describes the physical propagating particle well in both cases, as its negative square is the same as the sampled Q^2. The parton four-vectors $\hat{p}$ and $\hat{p}'$ on the other hand might not describe the quark well enough in the lower end of the phase space, since the reconstructed x differs slightly from the sampled x.

PYTHIA assumes initial state particles to be massless, and final state particles massive. Inclusion of lepton mass has no effect in results of the presented simulation.

The effect of adding the quark masses is most noticeable in the missing mass distribution of figure 10. The massless case somewhat agrees with the results from PYTHIA, but adding quark masses results in a different shape for the W graph. Differences in the inelasticity y and transverse momentum $\hat{p}'_{\mathrm{T}}$ distributions (figures 11 and 12) are minor and more noticeable when plotted in a logarithmic y-axis. The gathered results imply that the sampling of x and Q^2 is working as intended, but another way to build the kinematics may be beneficial to get better results with massive quarks.

Overall, the gathered distributions with massless quarks seemed to agree better with PYTHIA's distributions. This is no surprise, as PYTHIA doesn't handle all masses in the events either. However, building the kinematics in a consistent way to preserve the sampled quantities and four-momenta proved to be a difficult task when the quark masses are added to the simulation.

The improvements to existing PYTHIA event generation were to include quark masses and preserve the sampled quantities when calculated from the constructed four-vectors. The created simulation program has these features, but building the kinematics with massive quarks introduced some unwanted behaviour in the results. The program only handles the parton level sub-process, with only the lepton and quark present in the final state. Some effort is still needed to finalize a suitable component for PYTHIA. Possible further improvements are the inclusion of charged-current interactions via a $W^{\pm}$ boson exchange, a different approach at building the kinematics as to preserve all wanted quantities, and hadronization processes to produce different final state particles.

References

[1] H. Abramowicz et al. "Combination of measurements of inclusive deep inelastic $e^{\pm}p$ scattering cross sections and QCD analysis of HERA data". In: *Eur. Phys. J. C* 75.12 (2015), p. 580. DOI: 10.1140/epjc/s10052-015-3710-4. arXiv: 1506.06042 [hep-ex].

[2] P. Agostini et al. "The Large Hadron-Electron Collider at the HL-LHC". working paper or preprint. Aug. 2020. URL: https://hal.archives-ouvertes.fr/hal-02917230.

[3] H. W. Kendall. "Deep inelastic scattering: Experiments on the proton and the observation of scaling". In: *Rev. Mod. Phys.* 63 (3 July 1991), pp. 597–614. DOI: 10.1103/RevModPhys.63.597. URL: https://link.aps.org/doi/10.1103/RevModPhys.63.597.

[4] T. Sjöstrand, S. Mrenna, and P. Skands. "PYTHIA 6.4 physics and manual". In: *Journal of High Energy Physics* 2006.05 (May 2006). ISSN: 1029-8479. DOI: 10.1088/1126-6708/2006/05/026. URL: http://dx.doi.org/10.1088/1126-6708/2006/05/026.

[5] C. Bierlich et al. *A comprehensive guide to the physics and usage of PYTHIA 8.3*. 2022. DOI: 10.48550/ARXIV.2203.11601. URL: https://arxiv.org/abs/2203.11601.

[6] *PYTHIA Welcome page*. pythia.org. Visited: 12.4.2022.

[7] M. Tanabashi et al. "Review of Particle Physics". In: *Phys. Rev. D* 98 (3 Aug. 2018), p. 030001. DOI: 10.1103/PhysRevD.98.030001. URL: https://link.aps.org/doi/10.1103/PhysRevD.98.030001.

[8] A. Buckley et al. "LHAPDF6: parton density access in the LHC precision era". In: *The European Physical Journal C* 75.3 (Mar. 2015). DOI: 10.1140/epjc/s10052-015-3318-8. URL: https://doi.org/10.1140%2Fepjc%2Fs10052-015-3318-8.

[9] R. D. Ball et al. “Parton distributions with QED corrections”. In: *Nuclear Physics B* 877.2 (Dec. 2013), pp. 290–320. DOI: 10.1016/j.nuclphysb.2013.10.010. URL: https://doi.org/10.1016%2Fj.nuclphysb.2013.10.010.

[10] T. Sjöstrand et al. “An introduction to PYTHIA 8.2”. In: *Computer Physics Communications* 191 (June 2015), pp. 159–177. ISSN: 0010-4655. DOI: 10.1016/j.cpc.2015.01.024. URL: http://dx.doi.org/10.1016/j.cpc.2015.01.024.

[11] J. I. Friedman. “Deep inelastic scattering: Comparisons with the quark model”. In: *Rev. Mod. Phys.* 63 (3 July 1991), pp. 615–627. DOI: 10.1103/RevModPhys.63.615. URL: https://link.aps.org/doi/10.1103/RevModPhys.63.615.

Fermion f	e	u, c, t	d, s, b
Weak isospin z-component T^3	-1	1	-1
Electromagnetic charge Q_f	-1	$2/3$	$-1/3$
Lefthanded Z vertex factor L_f	$-1 + 2\sin^2\theta_W$	$1 + -\frac{4}{3}\sin^2\theta_W$	$-1 + \frac{2}{3}\sin^2\theta_W$
Righthanded Z vertex factor R_f	$2\sin^2\theta_W$	$-\frac{4}{3}\sin^2\theta_W$	$\frac{2}{3}\sin^2\theta_W$
Weinberg angle $\sin^2\theta_W$	0.22278	Proton mass M	0.93827 GeV
Z boson coupling constant g_Z	0.017537	Electron mass m_e	0.000511 GeV
Fine-structure constant α	0.00729735	Z boson mass M_Z	91.1876 GeV

Table 1. Coupling constants and other physical constants.

A Feynman rules and physical constants

Table 1 holds the relevant physical constants used in the simulation. The Z boson vertex factors for fermion f are given by

$$L_f = T_f^3 - 2Q_f \sin^2\theta_W \qquad R_f = -2Q_f \sin^2\theta_W. \tag{77}$$

A.1 Interaction vertices

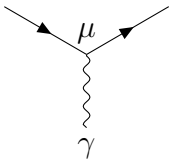

$= iQ_f e\gamma^\mu$

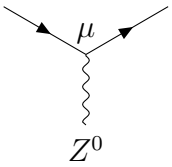

$= -ig_z\gamma^\mu[L_f(1-\gamma^5) + R_f(1+\gamma^5)]$ (78)

A.2 Boson propagators

$\mu \quad \gamma \quad \nu = \frac{-ig_{\mu\nu}}{q^2+i\epsilon}$ $\mu \quad Z^0 \quad \nu = \frac{-i}{(q^2-M^2)+i\epsilon}[g_{\mu\nu} - \frac{q^\mu q^\nu}{M^2}]$ (79)

A.3 External legs

 $= u^s(p)$ Incoming fermion

 $= \overline{u}^s(p)$ Outgoing fermion

 $= \overline{v}^s(p)$ Incoming antifermion

 $= v^s(p)$ Outgoing antifermion (80)

GitLab-page of the simulation project: `https://gitlab.jyu.fi/joollaul/dis-mc-simulation-pro-gradu/`

B Tensor contractions

The contraction $L^{\mu\nu}_{\gamma} W^{\gamma}_{\mu\nu}$ is calculated as follows. The leptonic tensor (19) is fully symmetric, so the contraction is non-zero only for the symmetric part of $W^{\gamma}_{\mu\nu}$. Using the following equalities

$$q = k - k' \qquad q^2 = \cancelto{0}{k^2} + \cancelto{0}{k'^2} - 2(k \cdot k'), \qquad (p \cdot q) = (p \cdot k) - (p \cdot k')$$
$$(k \cdot q) = \cancelto{0}{k^2} - (k \cdot k'), \qquad (k' \cdot q) = (k \cdot k') - \cancelto{0}{k'^2}$$

gives the contraction as

$$\begin{aligned}
L^{\mu\nu}_{\gamma} W^{\gamma}_{\mu\nu} &= 2\Big[k'^{\mu}k^{\nu} + k'^{\nu}k^{\mu} - (k \cdot k')g^{\mu\nu}\Big] \\
&\times \Big[- W^{\gamma}_1(g_{\mu\nu} - \frac{q_\mu q_\nu}{q^2}) + \frac{W^{\gamma}_2}{M^2}(p_\mu - \frac{(q \cdot p)}{q^2}q_\mu)(p_\nu - \frac{(q \cdot p)}{q^2}q_\nu)\Big] \\
&= -2W^{\gamma}_1[-(k \cdot k') - 2\frac{-(k \cdot q)(k' \cdot q)}{q^2}] + \frac{W^{\gamma}_2}{M^2}\Big[2(k \cdot p)(k' \cdot p) - (k \cdot k')p^2 \\
&- \frac{(p \cdot q)}{q^2}\Big(2(k \cdot p)(k' \cdot q) + 2(k \cdot q)(k' \cdot p) - 2(k \cdot k')(p \cdot q)\Big) \\
&+ \frac{(p \cdot q)^2}{q^4}\Big(2(k \cdot q)(k' \cdot q) - (k \cdot k')q^2\Big)\Big] \\
&= 4W^{\gamma}_1(k \cdot k') + 4\frac{W^{\gamma}_2}{M^2}\Big[(k \cdot p)(k' \cdot p) - \frac{(k \cdot k')p^2}{2} \\
&+ \frac{(p \cdot q)}{q^2}[(k \cdot k')(k' \cdot p) - (k \cdot k')(k \cdot p) + (p \cdot k)(k \cdot k') - (p \cdot k')(k \cdot k')] \\
&+ \frac{(p \cdot q)^2}{q^4}[-(k \cdot k')^2 + (k \cdot k')^2]\Big] \\
&= 4\Big[W^{\gamma}_1(k \cdot k') + \frac{W^{\gamma}_2}{M^2}\Big((k \cdot p)(k' \cdot p) - \frac{(k \cdot k')p^2}{2}\Big)\Big]. \qquad (81)
\end{aligned}$$

The contractions of $L^{\mu\nu}_{Z} W^{Z}_{\mu\nu}$ and $L^{\mu\nu}_{\gamma Z} W^{\gamma Z}_{\mu\nu}$ are done similarly. They can be separated into symmetric and antisymmetric parts to ease the calculations, since contracting

symmetric and antisymmetric parts gives zero.

$$
\begin{aligned}
(L_Z^{\mu\nu})^S(W_{\mu\nu}^Z)^S &= 4(L_e^2+R_e^2)[k^\mu k'^\nu + k^\nu k'^\mu - (k\cdot k')g^{\mu\nu}] \\
&\times [-W_1^Z(g_{\mu\nu}-\frac{q_\mu q_\nu}{q^2}) + \frac{W_2^Z}{M^2}(p_\mu - \frac{(q\cdot p)}{q^2}q_\mu)(p_\nu - \frac{(q\cdot p)}{q^2}q_\nu)] \\
&= 8(L_e^2+R_e^2)[W_1^Z(k\cdot k') + \frac{W_2^Z}{M^2}((k\cdot p)(k'\cdot p) - \frac{(k\cdot k')p^2}{2})].
\end{aligned}
$$

This is the same form as $2(L_e^2+R_e^2)L_\gamma^{\mu\nu}W_{\mu\nu}^\gamma$. For the antisymmetric part the result

$$
\epsilon^{\mu\nu\alpha\beta}\epsilon_{\mu\nu\gamma\delta} = -2(\delta_\gamma^\alpha\delta_\delta^\beta - \delta_\delta^\alpha\delta_\gamma^\beta) \tag{82}
$$

is used:

$$
\begin{aligned}
(L_Z^{\mu\nu})^A(W_{\mu\nu}^Z)^A &= 4(L_e^2-R_e^2)i\epsilon^{\alpha\mu\beta\nu}k_\alpha k'_\beta \times (-\frac{W_3^Z}{2M^2}i\epsilon_{\mu\nu\gamma\delta}p^\gamma q^\delta) \\
&= -4(L_e^2-R_e^2)\frac{W_3^Z}{2M^2}[-2(\delta_\gamma^\alpha\delta_\delta^\beta - \delta_\delta^\alpha\delta_\gamma^\beta)k_\alpha k'_\beta p^\gamma q^\delta] \\
&= 4(L_e^2-R_e^2)\frac{W_3^Z}{M^2}[(k\cdot p)(k'\cdot q) - (k\cdot q)(k'\cdot p)] \\
&= 4(L_e^2-R_e^2)\frac{W_3^Z}{M^2}(k\cdot k')[(k\cdot p) + (k'\cdot p)] \\
&= -8(L_e^2-R_e^2)\frac{W_3^Z}{2M^2}\frac{q^2}{2}[(k\cdot p) + (k'\cdot p)].
\end{aligned}
$$

Similarly for the γZ part

$$
\begin{aligned}
(L_{\gamma Z}^{\mu\nu})^S(W_{\mu\nu}^{\gamma Z})^S &= 4(L_e+R_e)[W_1^{\gamma Z}(k\cdot k') + \frac{W_2^{\gamma Z}}{M^2}((k\cdot p)(k'\cdot p) - \frac{(k\cdot k')p^2}{2})] \\
(L_{\gamma Z}^{\mu\nu})^A(W_{\mu\nu}^{\gamma Z})^A &= -4(L_e-R_e)\frac{W_3^{\gamma Z}}{2M^2}\frac{q^2}{2}[(k\cdot p) + (k'\cdot p)].
\end{aligned}
$$